Journal of Pharmaceutical Analysis 15 (2025) 101068

Contents lists available at ScienceDirect

Journal of Pharmaceutical Analysis

journal homepage: www.elsevier.com/locate/jpa

Original article

Ursodeoxycholic acid inhibits the uptake of cystine through SLC7A11 and impairs *de novo* synthesis of glutathione

Fu'an Xie [a, 1], Yujia Niu [b, 1], Xiaobing Chen [c, 1], Xu Kong [a, 1], Guangting Yan [a], Aobo Zhuang [a], Xi Li [d], Lanlan Lian [e], Dongmei Qin [a], Quan Zhang [f], Ruyi Zhang [a], Kunrong Yang [g], Xiaogang Xia [h], Kun Chen [h], Mengmeng Xiao [i], Chunkang Yang [j], Ting Wu [a, c], Ye Shen [k, *], Chundong Yu [b, **], Chenghua Luo [i, ***], Shu-Hai Lin [b, ****], Wengang Li [a, h, *****]

[a] *Cancer Research Center, Xiang'an Hospital of Xiamen University, School of Medicine, Xiamen University, Xiamen, Fujian, 361102, China*
[b] *State Key Laboratory of Cellular Stress Biology, School of Life Sciences, Faculty of Medicine and Life Sciences, Xiamen University, Xiamen, Fujian, 361102, China*
[c] *Department of Retroperitoneal Tumor Surgery, Peking University International Hospital, Beijing, 102206, China*
[d] *School of Public Health, Harvard University, Boston, MA, 02115, USA*
[e] *Department of Laboratory Medicine, Xiang'an Hospital of Xiamen University, Xiamen University, Xiamen, Fujian, 361102, China*
[f] *National Institute for Data Science in Health and Medicine, Xiamen University, Xiamen, Fujian, 361102, China*
[g] *Laboratory of Biochemistry and Molecular Biology Research, Department of Clinical Laboratory, Fujian Medical University Cancer Hospital, Fujian Cancer Hospital, Fuzhou, 350014, China*
[h] *Department of Hepatobiliary Surgery, Xiang'an Hospital of Xiamen University, School of Medicine, Xiamen University, Xiamen, Fujian, 361102, China*
[i] *Department of General Surgery, Peking University People's Hospital, Beijing, 100032, China*
[j] *Department of Gastrointestinal Surgical Oncology, Fujian Medical University Cancer Hospital, Fujian Cancer Hospital, Fuzhou, 350014, China*
[k] *Department of Management, Jiang Xia Blood Technology Co., Ltd., Shanghai, 200000, China*

A R T I C L E I N F O

Article history:
Received 19 March 2024
Received in revised form
18 July 2024
Accepted 3 August 2024
Available online 22 August 2024

Keywords:
UDCA
SLC7A11
Cystine
GSH
Oxidative stress
RLPS

A B S T R A C T

Ursodeoxycholic acid (UDCA) is a naturally occurring, low-toxicity, and hydrophilic bile acid (BA) in the human body that is converted by intestinal flora using primary BA. Solute carrier family 7 member 11 (SLC7A11) functions to uptake extracellular cystine in exchange for glutamate, and is highly expressed in a variety of human cancers. Retroperitoneal liposarcoma (RLPS) refers to liposarcoma originating from the retroperitoneal area. Lipidomics analysis revealed that UDCA was one of the most significantly down-regulated metabolites in sera of RLPS patients compared with healthy subjects. The augmentation of UDCA concentration (≥25 μg/mL) demonstrated a suppressive effect on the proliferation of liposarcoma cells. [$^{15}N_2$]-cystine and [$^{13}C_5$]-glutamine isotope tracing revealed that UDCA impairs cystine uptake and glutathione (GSH) synthesis. Mechanistically, UDCA binds to the cystine transporter SLC7A11 to inhibit cystine uptake and impair GSH de novo synthesis, leading to reactive oxygen species (ROS) accumulation and mitochondrial oxidative damage. Furthermore, UDCA can promote the anti-cancer effects of ferroptosis inducers (Erastin, RSL3), the murine double minute 2 (MDM2) inhibitors (Nutlin 3a, RG7112), cyclin dependent kinase 4 (CDK4) inhibitor (Abemaciclib), and glutaminase inhibitor (CB839). Together, UDCA functions as a cystine exchange factor that binds to SLC7A11 for antitumor activity, and SLC7A11 is not only a new transporter for BA but also a clinically applicable target for UDCA. More importantly, in combination with other antitumor chemotherapy or physiotherapy treatments, UDCA may provide effective and promising treatment strategies for RLPS or other types of tumors in a ROS-dependent manner.

Peer review under responsibility of Xi'an Jiaotong University.
* Corresponding author.
** Corresponding author.
*** Corresponding author.
**** Corresponding author.
***** Corresponding author. Cancer Research Center, Xiang'an Hospital of Xiamen University, School of Medicine, Xiamen University, Xiamen, Fujian, 361102, China.
E-mail addresses: jerry.shen@delpstroke.com (Y. Shen), cdyu@xmu.edu.cn (C. Yu), luochenghua@pkuih.edu.cn (C. Luo), shuhai@xmu.edu.cn (S.-H. Lin), lwgang@xmu.edu.cn (W. Li).
[1] These authors contributed equally to this work.

https://doi.org/10.1016/j.jpha.2024.101068

1. Introduction

Primary bile acids (BAs) are primarily produced by liver cells. These primary BAs undergo transformations facilitated by the intestinal flora, resulting in the production of various forms of secondary BAs. This process is mainly carried out in the intestinal tract by *Clostridium mucricum, Clostridium inharmonious, Clostridium pasteuri*, and *Maltophilomonas*, accounting for 3%–4% of the total BA in the human body. The secondary BAs are predominantly conjugated with sodium and potassium salts, as well as taurine and glycine [1]. Ursodeoxycholic acid (UDCA), one of the most hydrophilic and least toxic BAs, has been widely used at a dosage of 10 mg/kg/day for treating gallstones [2], 22 mg/kg/day for primary biliary cholangitis [3], and as a preventive measure against severe acute respiratory syndrome coronavirus 2 (SARS-CoV-2) infection at dosages of 15 mg/kg/day for humans, 416 mg/kg/day for hamsters, and 1% w/w/day for mice [4]. In recent years, studies have reported that UDCA induces tumor cell death in several cancers, such as oral squamous carcinoma cells (400 μg/mL) [5], hepatocellular carcinoma cells (1.2 mM) [6], and gastric carcinoma cells (1 mM) [7]. The main molecular pathways and signal molecules implicated in the anticancer effects of UDCA involve signal transducer and activator of transcription 3 (STAT3), nuclear factor kappa-B (NFκB), extracellular signal-regulated kinase (ERK), p53, and reactive oxygen species (ROS) mediated by membrane receptors DR4/5 and Takeda G-protein-coupled receptor 5 (TGR5). Apoptosis was found to be the main type of cancer cell death induced by UDCA [8].

Cysteine serves as the precursor for glutathione (GSH), which is widely recognized as the predominant antioxidant in cells [9]. Cysteine is primarily derived from cystine, which is transported extracellularly by the cystine/glutamate antiporter system (system Xc-) [10]. In addition to extracellular uptake, mammalian cells can synthesize new cysteine through sulfurization using intracellular glucose and methionine [11]. Most cancer cells rely on the system Xc- to import cystine, which is then converted to cysteine through an nicotinamide adenine dinucleotide phosphate hydrogen (NADPH)-dependent reaction. The system Xc-functions as an electrically neutral and non-Na^+-dependent amino acid transporter, consisting of the 12-stage transmembrane transporter SLC7A11 and the single-stage transmembrane regulatory protein SLC3A2. The transport function of the system Xc- is mainly carried out by SLC7A11 [12]. SLC7A11 has close associations with various clinical diseases including acute organ injury, and age-related macular degeneration, and it has been found to be highly expressed in a variety of malignant tumors. Cystine reduction in the cytoplasm or inhibition of SLC7A11 can inhibit tumor cell proliferation and enhance their sensitivity to chemo-radiotherapy [13]. Many drugs are involved in regulating the SLC7A11 signaling pathway. HG106 [14], erastin, imidazole ketone erastin [15], sulfasalazine [16], and sorafenib [17] have been identified as SLC7A11 inhibitors that block cystine uptake. It is a pity that imidazole ketone erastin and HG106 have not yet progressed to clinical trials stage, except for sulfasalazine and sorafenib which are currently being used for arthritis treatment and human cancer treatment respectively after receiving approval from the U.S. Food and Drug Administration (FDA). Despite preclinical studies targeting SLC7A11 in cancer therapy, there is still an urgent need to further explore potent and specific inhibitors of SLC7A11, understand their underlying mechanisms, and eventually apply them in clinical studies.

Sarcomas represent a class of rare and highly heterogeneous malignant tumors of mesenchymal origin that can occur at any histological site [18]. There are over 100 different histological subtypes, mainly divided into three categories: soft tissue sarcoma, visceral sarcoma, and bone sarcoma. Retroperitoneal soft tissue sarcoma (RPS) accounts for 12%–15% of all soft tissue sarcoma (STS) [19], with liposarcoma being the most common pathological type. RPS is more likely to form large tumors and invade multiple adjacent organs. For patients with unresectable or metastatic dedifferentiated liposarcoma (DDLPS), anthracycline-based doxorubicin or doxorubicin in combination with ifosfamide is recommended as first-line chemotherapy [20]. Gemcitabine, either alone or in combination with docetaxel, vinorelbine, or dacarbazine, is often recommended for subsequent lines of chemotherapy [21]. However, after with complete resection, retroperitoneal sarcomas have a poor prognosis, with a recurrence rate of over 50% [22]. Therefore, it becomes imperative to develop novel potential therapeutics as alternative approaches to surgery for RPS.

In this study, we conducted mass spectrometry-based lipidomics and identified UDCA as one of the most downregulated metabolites in the sera of retroperitoneal liposarcoma (RLPS) patients compared to healthy subjects. We assumed that UDCA could be absorbed by large liposarcoma tissue volumes. Further investigation revealed whether and how UDCA can be utilized for RLPS treatment, highlighting its therapeutic value and implications for treating RLPS or other types of tumors with UDCA beyond surgery.

2. Methods and materials

2.1. Clinical samples and animals

We collected matched pairs of frozen and fixed samples from both normal and tumor tissues of 89 patients with DDLPS or well-differentiated liposarcoma (WDLPS). We also obtained serum samples from patients and healthy volunteers. All the samples were collected from Xiang'an Hospital of Xiamen University and Peking University International Hospital. Fixed samples were transferred to Shanghai Outdo Biotech Co., Ltd. for tissue microarray assays. The frozen tissue samples and serum samples were prepared for metabolomics analysis, while tissues were used for Western blot assays. The protocols were reviewed and approved by the ethics committees of all participating institutions, including Xiang'an Hospital of Xiamen University (Approval numbers: XAHLL2021024, and XAHLL2023004) and Peking University International Hospital (Approval number: WA2020RW29). All participants were enrolled and anonymized after approval by the institutional review board. Written informed consent was obtained from all participants, except those who could not be contacted due to a lack of follow-up. In these cases, permission was granted by the institutional review boards at each participating institution to use existing tissue samples for research purposes. None of the samples used in this study came from patients who had opted out of participation.

Moreover, we also collected postoperative serum samples, tumor tissue, and normal adjacent adipose tissue from patients with RLPS. The cohort consisted of a total of 69 retroperitoneal DDLPS patients, 20 retroperitoneal WDLPS patients, and 89 healthy subjects. The clinical characteristics of the sample sets are presented in Table S1.

The 4–6 weeks old male athymic nude mice and C57BL/6 mice were obtained from the Laboratory Animal Center of Xiamen University. The animals were regularly checked by a certified veterinarian who was responsible for health monitoring, animal welfare supervision, and experimental protocols. All experimental procedures involving animals were conducted in accordance with the animal protocols approved by the Laboratory Animal Center of Xiamen University and the Ethics Committee of Xiamen University (Approval number: XMULAC20190114). The RLPS orthotopic xenograft mouse model was established by injecting 0.1 mL of a tumor cell suspension containing 1×10^7 SW872 cells into the subcutaneous space. UDCA, cystine, and CB839 were administered

through intraperitoneal injection. Tumor growth was measured once every two days, and tumor volume (V) was calculated using the following equation: $V = (L \times W^2) \times 0.52$, where L is the length and W is the width of the xenograft. Once the length reaching a palpable size (2 cm), mice were euthanized under ether anesthesia, tumors were excised and weighed, and xenografted mice were divided into four groups: control group, UDCA (250 mg/kg daily) group, cystine (1 mmol/kg daily) group, and UDCA (250 mg/kg daily) plus cystine (1 mmol/kg daily) group. Each experimental group consisted of either five or seven mice. For *in situ* xenograft mouse model, we transplanted the liposarcoma cell line SW872 into the perirenal space of athymic nude mice to establish a mouse model of retroperitoneal sarcoma.

2.2. Cell lines and regents

SW872 (HTB-92), 93T449 (CRL-3043), 94T778 (CRL-3044), HT1080 (CCL-121), and MCF7 (HTB-22) cell lines were purchased from ATCC (Rockville, MD, USA). A549 (IM-H113), HCT116 (IM-H098), QBC939 (IM-H226), HUH7 (IM-H040), KYSE30 (IM-H311), MC38 (IM-M006) cell lines and basic medium were purchased from Xiamen Immocell Biotechnology Co., Ltd (Xiamen, Fujian, China). XMU-RC-1 and XMU-RC-2 cell lines were obtained from the Xiamen University Research Center of the Retroperitoneal Tumor Committee of the Oncology Society of the Chinese Medical Association (Xiamen, Fujian, China). SW872, XMU-RC-1, and XMU-RC-2 cells were cultured in Dulbecco's modified Eagle's medium (DMEM; SH30022.01, HyClone, Logan City, UT, USA) containing penicillin, streptomycin (SV30010, HyClone), and 10% fetal bovine serum (FBS; P30-3302, PAN, Edenbach, Baggolia State, Germany). 93T449 and 94T778 cells were cultured in RPMI-1640 medium (SH30255.01, HyClone) containing penicillin, streptomycin (SV30010, HyClone), and 10% FBS. UDCA (700199P) and dichloroacetic acid (DCA; 30960) were purchased from Sigma (Darmstadt, Germany). Tauroursodeoxycholic acid (TDCA) (HY-19696), RSL3 (HY-100218A), erastin (HY-15763), RG7112 (HY-10959), nutlin-3a (HY-10029), abemaciclib (HY-16297A), and CB839 (HY-12248) were purchased from MedChemExpress (Monmouth Junction, NJ, USA). Antibodies were purchased from the following sources: CD36 (10752-RP02, SinoBiological, Beijing, China), glyceraldehyde-3-phosphate dehydrogenase (GAPDH; TA-08, ZSGB-BIO, Beijing, China), GPX4 (ab125066, Abcam, Cambridge, UK), SLC7A11 (ab37185, Abcam), MDM2 (ab259265, Abcam), and P53 (2524S, Cell Signaling Technology, Danvers, MA, USA). LentiCRISPR v2-sgSLC7A11/xCT-2 (#161819) and Plenti6-SLC7A11/xCT-V5 (#170427) were purchased from Addgene (Cambridge, MA, USA). Cell counting kit-8 kit (RM02823) and C11 BODIPY 581/591 kit (RM02821) were purchased from Abclonal (Wuhan, China). Intracellular ROS production assay kit (DCFH-DA)) kit (S0033S) was purchased from Beyotine (Shanghai, China). Malondialdehyde (MDA) kit (ab118970) was purchased from Abcam(ab118970, Cambridge, UK).

2.3. Quantification and statistical analysis

Metabolomic data were imported into the online software MetaboAnalyst (https://www.metaboanalyst.ca/) for multivariate statistical analysis. For the metabolic flux data, the natural abundance correction of ^{15}N and ^{13}C for tracer experiments was performed with AccuCor (https://github.com/XiaoyangSu/AccuCor). Unless otherwise noted, statistically significant differences were assessed by a two-tailed Student's *t*-test. Graphs were prepared using GraphPad Prism 7.0. Data were presented as mean ± standard error of the mean (SEM). A *P*-value < 0.05 was considered statistically significant. The pan-cancer analysis is conducted using online software (http://www.sangerbox.com/home.html), where genes are entered into the search bar and the results of the pan-cancer analysis are automatically generated.

2.4. Cell counting kit-8 (CCK-8) assay and cell viability assay

The proliferation of cells was detected using a cell counting kit-8 (RM02823, Abclonal, Wuhan, China) assay following the manufacturer's instructions. 1,000 cells were inoculated in a 96-well plate and cultured at 37 °C and 5% CO_2. Then, 10 μL of CCK8 solution was added to each well and the plate was incubated for 1–4 h every two days. Finally, the absorbance at 450 nm was measured using a Microplate reader (Tecan spark, Mannedorf, Switzerland).

2.5. Reactive oxygen species assay kit (DCFH-DA)

5×10^4 cells were inoculated in 96-well plates and treated with UDCA and dimethyl sulfoxide (DMSO) for 6 h respectively. 2',7'-Dichlorodihydrofluorescein diacetate (DCFH-DA) was diluted in serum-free medium at a final concentration of 10 μM by a dilution ratio of 1:1000. The culture medium was removed, and then 100 μL of the diluted DCFH-DA was added. The cells were incubated at 37 °C for 20 min in the cell incubator. After that, the cells were washed three times with serum-free medium. Finally, the fluorescence intensity was detected using a fluorescence microplate reader (Varioskan Flash, Thermo Fisher Scientific, Waltham, MA, USA) under an excitation wavelength of 488 nm and an emission wavelength of 525 nm.

2.6. Lipid peroxidation assay (MDA)

The lipid peroxidation assay kit (ab118970, Abcam) was used to measure forms of reactive aldehydes such as MDA. Approximately 1×10^7 cells were harvested for each assay by washing with a cold phosphate buffered saline (PBS) solution. A lysis solution consisting of 300 μL MDA lysis buffer and 3 μL butylated hydroxytoluene (BHT) stock was mixed using a homogenizer on ice. The samples were then sonicated and centrifuged at 13,000 *g* for 10 min to collect the supernatant. To analyze the samples, 200 μL standard and 200 μL sample were added into vials or wells, followed by adding 600 μL developer VII/TBA reagent. After incubating at 95 °C for 60 min and cooling down, a reaction mix of 200 μL was transferred into a 96-well microplate for analysis. The absorbance at OD532 nm was immediately measured for colorimetric assay.

2.7. Lipid ROS assay (C11 BODIPY 581/591)

2×10^6 cells were inoculated into 6-well plates and treated with UDCA and DMSO for 6 h, respectively. The cells were then resuspended in 500 μL of PBS containing 20 mM C11-BODIPY 581/591 and incubated at 37 °C in a cell culture incubator for 1 h. The signals from both non-oxidized C11 (wavelength > 580 nm) and oxidized C11 (wavelength range: 505–550 nm) were monitored by flow cytometer (Cytoflex LX, Beckman Coulter, Pasadena, California, USA). The data were normalized to the control samples as indicated by relative lipid peroxidation.

2.8. Seahorse analysis

Oxygen consumption rates (OCR) were investigated using a Seahorse XFe96 Extracellular Flux Analyzer (Agilent Technologies, Boston, MA, USA). SW872 cells were washed and resuspended in OCR medium (Seahorse XF DMEM with 10 mM glucose, 2 mM glutamine, and 1 mM sodium pyruvate). A total of 2×10^4 cells were seeded in unbuffered culture medium in XFe96 Cell Culture

Microplates (101085-004, Agilent). After the initial assessment of basal OCR rates, modulators of mitochondrial function were sequentially injected at optimized concentrations using a standard mitochondrial stress test paradigm. For measurements of mitochondrial respiration rate, oligomycin A was added at a concentration of 1 μM followed by carbonyl cyanide-p-trifluoromethoxyphenylhydrazone (FCCP) at a concentration of 1 μM and rotenone (Rot)/antimycin A (AA) at a concentration of 1 μM.

2.9. Plasma sample preparation for metabolomics and lipidomics

For large-scale targeted metabolomics, the sera of 10 patient samples and 10 healthy samples were analyzed. 200 μL of acetonitrile was added to each 100 μL of serum sample and mixed with internal standard ([Ring-D_5]-phenylalanine solution), vortexed for 15 min at 4 °C, and stored at 4 °C for 2 h. After centrifugation at 14,000 *g* for 15 min at 4 °C, the supernatant was removed to a new tube and evaporated to dryness using a Labconco CentriVap (Labconco, Kansas, MO, USA). Metabolites were reconstituted in 100 μL of acetonitrile: water (1:1, *v/v*) with 0.1% formic acid, vortexed and centrifuged at 14,000 *g* for 15 min at 4 °C. The supernatant was subjected into liquid chromatography tandem mass spectrometry (LC-MS/MS. A quality control sample was generated by pooling all 20 sera samples and injecting it every 8−15 sample injections to monitor the consistency of the retention time and the signal intensity.

For lipidomics analysis, sera were thawed on ice, vortexed for approximately 10 s, and then centrifuged it at 3,000 rpm at 4 °C for 5 min. Serum (50 μL) was treated with 20 vol (1,000 μL) of solvent mixture (MTBE: methanol (3:1 *v/v*)) with internal standards (12:0 Lyso PC, Cer (d18:1/4:0) and PC (13:0/13:0)). After vortexing the mixture for 15 min, 200 μL of water was added and vortexed for 1 min, and the mixture was centrifuged at 12,000 rpm at 4 °C for 10 min. Then, 500 μL of the supernatant was evaporated under nitrogen to dryness. The dry extracts were reconstituted in 200 μL acetonitrile/isopropanol (1:9, *v/v*) with 0.1% formic acid and 10 mM ammonium formate before analysis. A quality control sample was generated by pooling all 20 plasma samples and injecting it every 8−15 sample injections to monitor the consistency of the retention time and the signal intensity.

The quantitative analysis of UDCA involved the classification of samples into two groups. Group 1 consisted of 53 patient samples and 53 normal samples. Group 2 included preoperative samples and corresponding postoperative samples from 16 patients. Serum (100 μL) was treated with 4 vol (400 μL) of methanol solvent with internal standards (D4-chenodeoxycholic acid), vortexed for 5 min, and incubated at 4 °C for 1 h to allow for protein precipitation. After centrifugation at 14,000 *g* for 15 min at 4 °C, the supernatant was pelleted by centrifugation at 4 °C, and the supernatant containing UDCA was collected and evaporated to dryness using a Labconco CentriVap. Metabolites were reconstituted in 50 μL of methanol:-water (4:1, *v/v*), vortexed, and centrifuged to remove insoluble material before analysis. To monitor the consistency of the retention time and the signal intensity, a quality control sample was generated by pooling all plasma samples and injecting it every 8−15 sample injections. To absolutely quantify the concentration of UDCA in serum, a UDCA standard curve was plotted. The UDCA standards were diluted to 0.1, 0.2, 0.5, 1, 5, 10, 20, 50, and 100 ppb separately.

2.10. Cells for metabolomics

Freshly enriched SW872 and XMU-RC1 cells were resuspended in cell culture medium RMPI 1640 medium containing 10% (*v/v*) 56 °C heat-inactivated fetal bovine serum and 1% (*v/v*) penicillin−streptomycin. A total of 1×10^6 cells were cultured in a flat-bottomed 6-well plate. Cells were cultured in a cell incubator at 37 °C with 5% CO_2. Following cell adherence, 400 μg/mL UDCA was added. After 6 h, the medium was removed, and cells were washed with room-temperature PBS twice to obtain cell pellets. A precooled 80% methanol solution was added to the cell pellets for metabolite extraction.

2.11. Cells for stable isotope tracing analysis

Freshly enriched SW872 cells were resuspended in medium as described above. After cell adherence, the medium was removed and washed with room-temperature PBS twice to obtain cell pellets. For [^{15}N]-cystine metabolic flux analysis, medium (RMPI 1640 medium (Shanghai Basal Media Technologies Co., Ltd., Shanghai, China; Customized, without cystine) containing 10% (*v/v*) 56 °C heat-inactivated dialyzed fetal bovine serum, 1% (*v/v*) penicillin−streptomycin, 0.21 mM [$^{15}N_2$]-cystine] and 400 μg/mL UDCA were added. Cell samples were collected at 3, 6, 12, and 24 h. For [U−^{13}C]-glutamine metabolic flux analysis, medium (RMPI 1640 medium (Shanghai Basal Media Technologies Co., Ltd.; Customized, without glucose or glutamine) containing 10% (*v/v*) 56 °C heat-inactivated dialyzed fetal bovine serum, 1% (*v/v*) penicillin−streptomycin, 2 mM [U−^{13}C]-glutamine, and 11.1 mM label-free glucose) and 400 μg/mL UDCA were added. Cell samples were collected at 1 h, 3 h, and 6 h. Precooled 80% methanol was added to the cell pellets for metabolite extraction.

2.12. LC-MS/MS for targeted metabolomics

LC-MS was performed using an Exion LC system (AB SCIEX, Boston, MA, USA) with a ZIC-pHILIC column (100 mm × 2.1 mm; Millipore, Bedford, MA, USA) connected to QTRAP-5500 mass spectrometer (AB SCIEX). For LC conditions, 2 μL samples were injected and analyzed. The flow rate was 0.2 mL/min. The column and tray temperature were set at 40 °C and 4 °C, respectively. The mobile phase A contained 15 mM ammonium acetate and 3 mL/L ammonium hydrate (>28%) in water, while mobile phase B was a 90% acetonitrile aqueous solution. The gradient elution was set as follows: the initial concentration of B was maintained at 95% for 1 min; decreased to 45% over 14 min and held at this level for 2 min; increased to 95% over 0.5 min and held at this level for 4.5 min. The electrospray ionization (ESI) voltage was set to 4,500 V in negative ion multiple reaction monitoring mode, and ion temperature and curtain gas were set at 500 °C and 35 μL/min. LC-MS/MS conditions were controlled by Analyst 1.7.1 software and the final data were processed by Mutiquant 3.0.3 software. To track GSH biosynthesis metabolic flux, [^{15}N2]-cystine was used in cell culture. The metabolite isotopologs were measured by LC-MS/MS analysis. Multiple reaction monitoring data of ^{15}N-labeled metabolite isotopologs were also acquired using Analyst software (version 1.6.3, AB SCIEX).

2.13. LC-MS/MS for lipid metabolomics

The supernatant was injected into a Thermo AccucoreTMC30 (2.1 mm × 100 mm, 2.6 μm; Thermo Fisher Scientific) column. The column temperature, flow rate, and injection volume were set to 45 °C, 0.35 mL/min, and 2 μL, respectively. The mobile phase consisted of acetonitrile:water (6:4, *v/v*) containing 0.1% formic acid and 10 mM ammonium formate (A) and acetonitrile:isopropanol (1:9, *v/v*) containing 0.1% formic acid and 10 mM ammonium formate (B). The gradient program was A:B (8:2, *v/v*) at 0 min, A:B (7:3, *v/v*) at 2 min, A:B (4:6, *v/v*) at 4 min, A:B (15:85, *v/v*) at 9 min,

A:B (1:9, *v/v*) at 14 min, A:B (5:95, *v/v*) at 15.5 min, held for 1.8 min and returned to A:B (80:20, *v/v*) at 20 min. Mass spectra were acquired on a SCIEX triple quadrupole-linear ion trap mass spectrometer (QTRAP) 6500+ LC-MS/MS system, equipped with an ESI Turbo ion spray interface, operating in positive and negative ion modes and controlled by Analyst 1.6.3 software (AB SCIEX). The ESI source temperature and ion spray voltage were set at 500 °C and 5,500 V (positive) and −4,500 V (negative), respectively. The ion source gas I, gas II, and curtain gas were set at 45, 55, and 35 psi, respectively.

2.14. Precipitation–LC-MS/MS assay

For the interaction of UDCA-SLC7A11 and cystine-SLC7A11, the cell lysate of SW872 cells was divided into eight groups (1 mg/mL, 1 mL/group). These groups underwent various treatments, including the blank control group, cystine treatment group, UDCA treatment group, UDCA-cystine co-treatment group, UDCA pretreatment (PTM) plus cystine group, and cystine PTM plus UDCA group. Immunoprecipitation was performed using an SLC7A11 antibody. Cell lysates were precipitated using Protein A/G Magnetic Beads (HY-K0202, MCE, Monmouth Junction, NJ, USA). After extensive washing, the precipitates were subjected to three rapid freeze-thaw cycles and cooled at 4 °C for 1 h. The samples were vortexed and centrifuged for 15 min at 14,000 *g* at 4 °C. The supernatants containing aqueous metabolites were collected by centrifugation at 4 °C and evaporated to dryness using a Labconco centriVap. Metabolites were reconstituted in 60 μL of acetonitrile:water (1:1, *v/v*) with 0.1% formic acid; then they were vortexed and centrifuged to remove insoluble material. LC-MS analysis was performed to analyze UDCA and cystine.

2.15. Precipitation assay

The cells were first lysed with a lysis buffer to assess the interaction of UDCA-EA-Biotin with SLC7A11. Then, the cell lysates were treated with an SLC7A11 antibody, control immunoglobulin, and UDCA-EA-biotin. Subsequently, the lysates were precipitated using Protein A/G Magnetic Beads (HY-K0202, MCE) and Streptavidin Magnetic Beads (HY-K0208, MCE). After extensive washing, the precipitates were analyzed by Western blotting analysis.

2.16. Immunohistochemical staining

Tissue sections underwent a dewaxing process using xylene, followed by a hydrated process using graded alcohol solutions and distilled water. Routine hematoxylin and eosin staining was carried out. Immunohistochemical staining was performed using antibodies against the proto-oncogene MDM2, which is commonly expressed in RLPS, the adipose tissue biomarker CD36, and SLC7A11, according to the manufacturers' recommendations. Sepia staining was considered positive staining. Tissue points were observed throughout the entire field, subsequently leading to the selection of three distinct fields exhibiting different staining intensity for interpretation. If the marker located in the cell nucleus, 100 cells were randomly recorded in each field, and the percentage of positive cells in 100 cells was recorded as X_1%. Similarly, the percentage of positive cells in the other two fields was recorded as X_2% and X_3%, respectively; then an average of these positive staining rates at this tissue location was taken. If the marker is located in cytoplasm or membrane, we also selected three different fields with varying staining intensities to estimate their respective positive rates and took their average value.

2.17. Western blotting detection

Liposarcoma cell lines and liposarcoma tissue from patients were lysed in radio immunoprecipitation assay lysis buffer (RIPA; P0013B, Beyotime, Shanghai, China), and the proteins were quantified using BCA assays (A55864, Thermo Fisher Scientific). Equal amounts of proteins were loaded onto 10% sodium dodecyl sulfate-polyacrylamide gel electrophoresis (SDS-PAGE) gels and transferred to polyvinylidene difluoride membranes, followed by immunoblotting with a specific antibody. The Western blots were analyzed using a Tanon Imager (Tanon 5200, Shanghai Tanon Science & Technology Co., Ltd., Shanghai, China).

2.18. Quantitative polymerase chain reaction (qPCR)

Total RNA was extracted using TRIzol regent (9109, Osaka, Japan) and underwent reverse transcription into cDNA using a cDNA synthesis kit (RR047, Takara, Osaka, Japan), according to the manufacturer's instructions. qPCR was conducted using SYBR GREEN (RR420, Takara). The primer sequences were as follows: h-β-actin-F-TCTTCCAGCCTTCCTTCCT, h-β-actin-R-AGCACTGTGTTGGCGTACAG; h-GLS1-F-AGGGTCTGTTACCTAGCTTGG, h-GLS1-R-ACGTTCGCAATCC TGTAGATTT; h-GLS2-F-GAAATTCGGAACAAGACTGTG, h-GLS2-R-AACTTCGATGTGTCCTTCAG.

2.19. Metabolite flux analysis

2.19.1. Labeling extent LE) calculation

LE represents the labeling enrichment of one metabolite:

$$LE = 1 - M_0$$

L_{M0} is the labeled fraction of M_0

2.19.2. Labeling kinetic flux profiling

We fitted the tracing kinetics of the isotopically labeled metabolites using the general first-order exponential equation for quantitation of the labeling rates of key metabolites.

$$LE = m \times e^{(-kt)} - m \quad (m < 0),$$

In this formula, k is the first-order rate constant, indicating the incorporation rate of the tracer to a metabolite target, and k and m were fitted using the R package “nls” from the LE values.

2.19.3. Metabolic flux analysis

Our lab made a mathematical model for calculation of metabolic flux in INCA software (Available at https://mfa.vueinnovations.com). In INCA environment, we use EMU, optimization, and Monte Carlo algorithms in solving fluxes.

3. Results

3.1. Decreased UDCA is observed in the sera of RLPS patients

To delineate the metabolic signature of RLPS, we enrolled RLPS patients to analyze their serum metabolome compared with sex- and age-matched healthy subjects without abnormal biochemical values or a history of tumors. We first measured serum lipid alterations between 10 DDLPS patients (5 males, 5 females; mean age = 48.2 ± 3.818) and 10 healthy individuals (5 males, 5 females; mean age = 41.7 ± 3.197) randomly using lipidomic analysis. The partial least squares-discriminant analysis (PLS-DA) mapping showed a clear separation between DDLPS patient samples and healthy control samples (Fig. 1A). A total of 756 lipids were

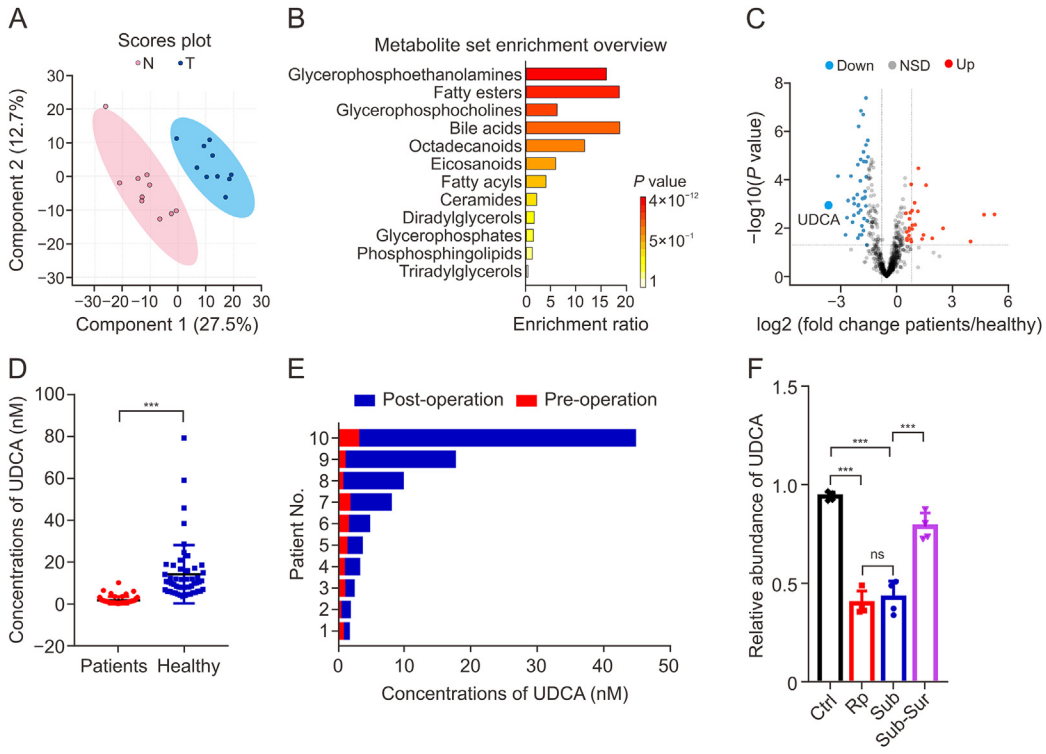

Fig. 1. Lipidomic analysis of serum samples from retroperitoneal liposarcoma (RLPS) patients and healthy donors. (A) Partial least squares discrimination analysis performed on the lipidomic data in both the healthy cohort and patients. $n = 10$ per group. N: normal healthy individuals; T: retroperitoneal dedifferentiated liposarcoma patients. (B) Kyoto Encyclopedia of Genes and Genomes (KEGG) functional enrichment analysis of the lipid levels. $n = 10$ per group. (C)The volcano plot of the relative abundance of lipids, where differentially expressed lipids are labeled in red (upregulated) and blue (downregulated). Decreased UDCA is observed in the sera of RLPS patients. $n = 10$ per group. NSD: no significant difference. (D) Absolute quantification of UDCA concentrations measured in both patients and healthy individuals using internal standards (D4-chenodeoxycholic acid). $n = 53$ per group. Data are presented as mean ± SEM. $^{***}P<0.0001$. (E) The concentration of UDCA in the pre-operation period and the post-operation period, determined by measuring it against internal standards (D4-chenodeoxycholic acid). $n = 10$. (F) Relative quantification of UDCA concentrations measured in liposarcoma-bearing mice after treatment with UDCA (200 mg/kg) for 24 h (Ctrl: no liposarcoma inoculation; Rp: liposarcoma was inoculated retroperitoneally; Sub: liposarcoma inoculated subcutaneously; Sub-Sur: liposarcoma inoculated subcutaneously and sarcoma removed by surgery). $n = 3$. Data are mean ± SEM. $^{***}P<0.001$; ns: not significance. Data were analyzed using two-tailed Student's *t*-tests.

identified using reference standards and LC/MS fragmentation by searching against our in-house database (Fig. S1, and Table S2). Next, we conducted pathway enrichment analysis using the Kyoto Encyclopedia of Genes and Genomes (KEGG) database and identified the significantly enriched pathways. Metabolite set enrichment analysis highlighted glycerophosphoethanolamines, fatty esters, glycerophosphocholines, BAs, and octadecanoids in the comparison of serum samples between RLPS patients and healthy subjects (Fig. 1B). Intriguingly, we found that UDCA was one of the most significantly decreased metabolites in the sera of patients with retroperitoneal DDLPS compared with healthy controls (Fig. 1C). By further analyzing serum BAs, we found that chenodeoxycholic acid (CDCA), a precursor of UDCA, was also significantly decreased in RLPS patients compared with healthy subjects (Fig. S2).

To confirm the changes of UDCA in sera, we conducted absolute quantification of UDCA in a larger cohort of RLPS patients ($n = 53$). As shown in Fig. 1D, a decreased UDCA concentration was observed in the sera of RLPS patients compared with healthy controls. We further asked whether surgery impacted the UDCA level in sera. Interestingly, we found that the UDCA concentration in the sera of postoperative patients was markedly higher than in the preoperative retroperitoneal DDLPS samples ($n = 10$ per group) (Fig. 1E). To verified the decreased UDCA in mice model, we inoculated nude mice with liposarcoma cells (SW872) subcutaneously and retroperitoneally. The mice were divided into four groups: no liposarcoma inoculation (Ctrl), liposarcoma inoculated subcutaneously (Sub), liposarcoma inoculated retroperitoneally (Rp), and liposarcoma inoculated subcutaneously with subsequent sarcoma removal by surgery (Sub-Sur). After intraperitoneal injection of UDCA at a dose of 200 mg/kg, the results showed that UDCA levels in serum were lower in the Rp group and Sub group compared to the Ctrl group. However, the UDCA level in the Sub-Sur group was higher than that in the Sub group (Fig. 1F), supporting our notion that there is a negative correlation between UDCA and liposarcomas as well as their development. Furthermore, it was observed that the location where the liposarcoma cells were transplanted on the mouse did not affect this correlation.

3.2. UDCA exhibits different functions depending on the concentrations

Based on the above results, we believe that UDCA is directly related to liposarcoma cells, so we wanted to understand the function of UDCA and why it decreases in the serum of RLPS patients. Previous studies have shown that UDCA has different effects at various concentrations: tumor cell studies *in vitro* (19.6–400 μg/mL) [23], clinical treatment of primary biliary cholangitis and cholestatic liver disease (10–20 mg/kg daily) [24,25], and the normal physiological concentration of UDCA in sera (0.0047–0.264 μg/mL) [26]. Therefore, we treated SW872 and 93T449 cells with varying concentrations of UDCA for 7 days (400, 200, 100, 50, 25, 6.25, 1.5625, 0.39063, 0.09766, 0.02441, 0.00610, 0.00153, 0.00038, 0 μg/mL). We observed that cell proliferation was inhibited by UDCA at concentrations greater than 25 μg/mL (Figs.

2A and B). Consequently, we focused more on the clinical value and targets of UDCA in anti-cancer therapy. We found that at concentrations greater than 400 μg/mL for 24 h, UDCA significantly induced cell death; however, at concentrations less than 200 μg/mL for 24 h, UDCA did not affect the viability of any tested cells (Fig. S3). BAs are amphipathic molecules. To rule out the possibility that this is a common characteristic of BAs, we administered DCA and TDCA at an equivalent concentration to treat SW872 cells and 93T449 cells. The results showed that the lethality of UDCA (400 μg/mL) was significantly higher than that of DCA (400 μg/mL) or TDCA (400 μg/mL) (Fig. S4). To verify the effect of UDCA on liposarcoma cell proliferation, colony formation assays were conducted, which found that UDCA (200 μg/mL) significantly inhibited cell proliferation rates compared to the vehicle groups (Figs. 2C–F and S5A and B). Transmission electron microscope (TEM) observations revealed notable changes in liposarcoma cells treated with UDCA: cytoplasmic dilatation was observed; the cytoplasmic membrane remained intact; the cytoplasmic vacuoles increased in size; the nuclear membrane appeared intact but electron-lucent; cristae in mitochondria reduced in number or even disappeared (Figs. 2G and H, and S5C, movies S1 and S2). Therefore, we suspected that UDCA-induced cell death was associated with oxidative stress and mitochondrial dysfunction. Next, ROS measurement using DCFH-DA revealed a substantial increase in ROS levels upon treatment with UDCA. Lipid peroxidation analysis using BODIPY showed an enrichment of lipid peroxidation in these cells. MDA levels were significantly increased in both SW872 and 93T449 cells when treated with UDCA at 400 μg/mL for 12 h (Fig. 2I–K, M–O). The morphology of SW872, 93T449, and XMU-RC-1 cells by TEM after stimulation with UDCA differed from typical apoptosis, necrosis, autophagy, ferroptosis, or pyroptosis patterns. Considering multiple studies reporting that UDCA regulates apoptosis, we examined changes in P53 after treatment with UDCA but found it to be downregulated in SW872, 93T449, and 94T778 cells (Fig. S6). Interestingly, RSL3 (1 μM) and erastin (10 μM) treatment induced more ferroptosis in both SW872 and 93T449 cells upon UDCA exposure (Figs. 2L and P, and S7).

Supplementary video related to this article can be found at https://doi.org/10.1016/j.jpha.2024.101068

3.3. UDCA treatment reprograms cellular metabolism and impairs GSH synthesis

To further elucidate the underlying targets and mechanisms of UDCA-mediated cell death, we performed targeted metabolomics analysis on both SW872 and XMU-RC-1 cells treated with UDCA (400 μg/mL, 6 h). The PLS-DA model clearly separated the vehicle and UDCA groups (Figs. 3A, and S8A). In the identified metabolites, amino acids, fatty acids, organic acids, carbohydrates, and other metabolites were included (Tables S3 and S4). Volcano plots and heatmaps showed downregulation of cysteine and GSH in all SW872 and XMU-RC-1 cells treated with UDCA (Figs. 3B and E, S8B and E, and S9). Alanine aspartate glutamate metabolism pathways were significantly altered in both cell lines (Figs. 3C, S8C, and S9). Additionally, metabolic pathway enrichment analysis using the KEGG database revealed significantly downregulated cystine and methionine metabolism pathways for both SW872 and XMU-RC-1 cells (Figs. 3D and S8D).

To gain a more comprehensive understanding of gene expression changes induced by UDCA-induced cell death, transcriptomics were performed to globally survey RNA level alterations upon UDCA treatment. We observed significant downregulation of cysteine and methionine metabolism in both SW872 and 93T449 cells (Fig. S10, and Table S5 and S6). These findings align with the targeted metabolomics analysis mentioned above.

To verify the metabolic reprogramming linked to cysteine and methionine metabolism in cells following UDCA treatment, we utilized [$^{15}N_2$]-cystine and [$^{13}C_5$]-glutamine, respectively, as tracers for stable isotope tracing respectively. Quantitative analysis of metabolic flux analysis of nitrogen incorporation in the intracellular ^{15}N-labeled cystine isotopomers [M2], GSH isotopomers [M1], and glutathione disulfide (GSSG) isotopomers [M2] showed that UDCA significantly reduced ^{15}N-enrichment in GSH biosynthesis (Figs. 4A–D). Additionally, the assessment of GSH labeling rate demonstrated a significant decrease in GSH synthesis after UDCA treatment (Figs. 4E and F). The levels of cystine in the culture medium decreased over time, however, the addition of UDCA did not affect cystine level in the culture medium (Fig. 4G).

Similarly, the fraction of GSH isotopomers [M5] and GSSG isotopomers [M10] derived from [$^{13}C_5$]-glutamine also decreased with UDCA treatment (Figs. 4H–L). It is worth noting that the glutamate isotopomer [M5] and the ratio of glutamate to glutamine increased after UDCA treatment (Fig. 4M), indicating an increase in endogenous glutamate levels in cells. We further demonstrated significant upregulation of GLS2 rather than GLS1 (Fig. S11). Additionally, we detected an increase in glutamate levels in the culture medium over time, which was significantly enhanced by the addition of UDCA compared to control conditions (Fig. 4N). Using [$^{13}C_5$]-glutamine as a tracer, we observed a significant decrease in citrate isotopomers [M4] and isocitrate isotopomers [M4] through oxidative metabolism following UDCA treatment, while citrate isotopomers [M5] and isocitrate isotopomers [M5] via reductive carboxylation were markedly increased (Figs. 4O and P). To further validate these findings and explore metabolic characteristics after UDCA-induced mitochondrial dysfunction, we investigated glucose metabolism using [1,2-$^{13}C_2$]-glucose as a tracer. As a result, we observed a significant decrease in citrate isotopomers [M2], isocitrate isotopomers [M2], α-KG [M2], succinate [M2], fumarate [M2], and malate [M2] through oxidative metabolism after UDCA treatment (Figs. 4Q and R). It should be noted that GSH can also be generated from GSSG using NADPH produced in the oxidative branch of the pentose phosphate pathway (oxPPP). After UDCA treatment, we observed a significant decrease in the isotopomers ribulose 5-phosphate (Ru5P) [M1] and ribose 5-phosphate (R5P) [M1] through oxPPP. Additionally, the ratio of ribose 5-phosphate [M1] to glucose 6-phosphate [M2] also decreased significantly, indicating a notable reduction in NADPH production via oxPPP (Fig. 4S and T), which corresponds to the depletion of GSH transformation from GSSG. Metabolic flux analysis was conducted using INCA [27], based on tracing with based on tracing with [1,2-$^{13}C_2$]-glucose isotope. The quantified metabolic fluxes revealed that the conversion rate of citrate to α-KG through oxidative metabolism was significantly higher in the DMSO group ($V_4 = 101.48$) compared to the UDCA group ($V_4 = 42.48$). However, the conversion rate of glutamate to α-KG was significantly lower in the DMSO group ($V_7 = 229.22$) compared to the UDCA group ($V_7 = 370.88$) (Figs. 4U and V). Collectively, these findings support that UDCA treatment impairs *de novo* synthesis of GSH, leading to increased oxidative stress and mitochondrial dysfunction in liposarcoma cells.

3.4. Cystine partially rescues UDCA-induced cell death, while CB-839 sensitizes liposarcoma cells to UDCA-induced cell death

Considering that UDCA exposure rearranges cellular metabolic networks to inhibit GSH *de novo* synthesis, we further investigated whether cystine can effectively rescue UDCA-induced cell death in both DDLPS and WDLPS. We treated different liposarcoma cell lines with UDCA (400 μg/mL) combined with varying concentrations of cystine. Our data indicated that cystine (10 mM) significantly rescued cell death in the tested cells (SW872, XMU-RC-1, 93T449,

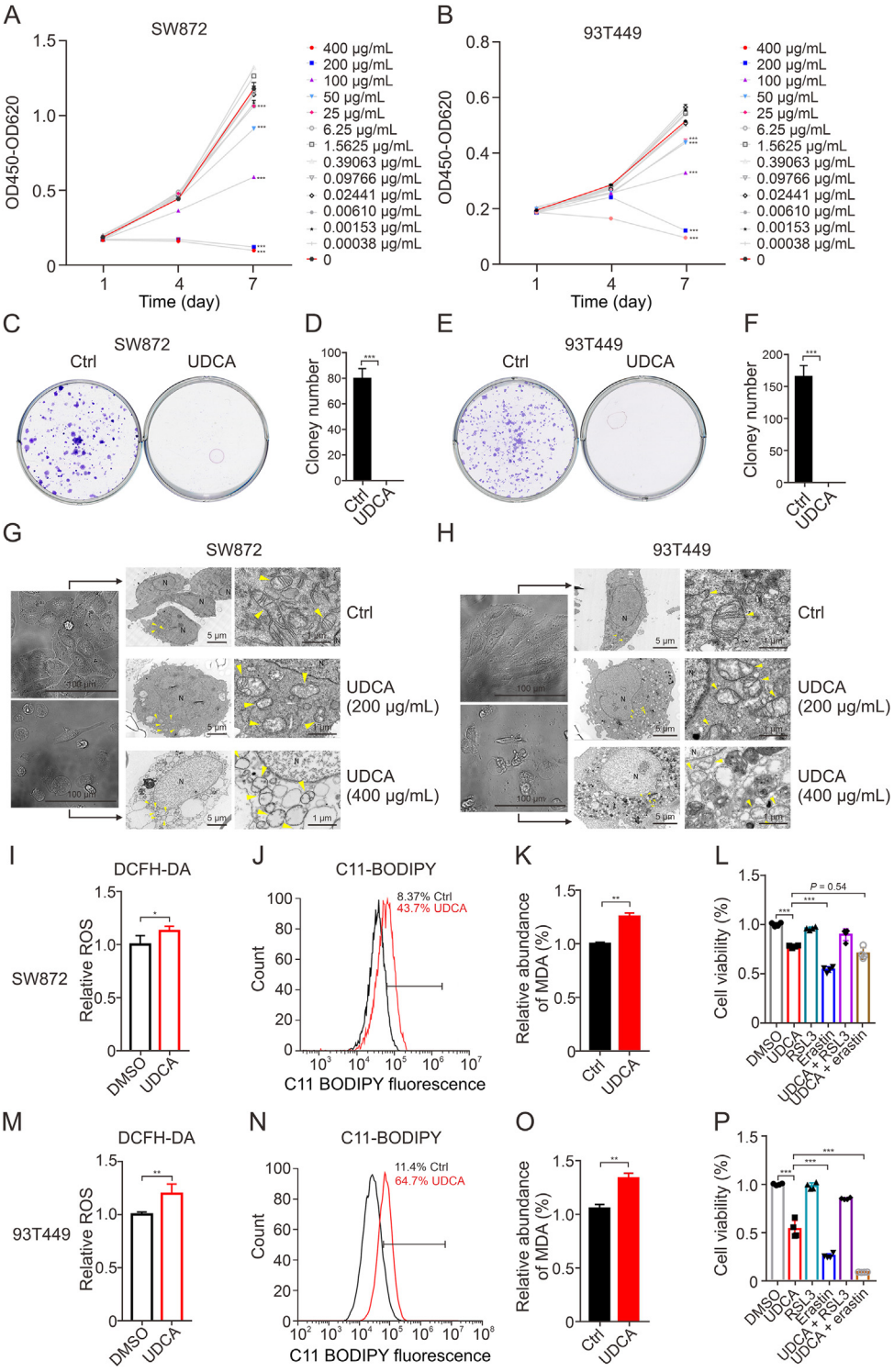

Fig. 2. UDCA suppresses the proliferation of liposarcoma cells and increases their sensitivity to ferroptosis. (A, B) Cell viability analyzed after treatment with different concentrations of UDCA (400, 200, 100, 50, 25, 6.25, 1.5625, 0.39063, 0.09766, 0.02441, 0.00610, 0.00153, 0.00038, 0 μg/mL) in SW872 (A) and 93T449 (B) cells. $n = 5$. (C–F) Treatment with UDCA (200 μg/mL) leading to reduced clone formation in SW872 (C, D) and 93T449 (E, F) cells. $n = 3$. Data are mean ± standard deviation (SD). $^{***}P$ <0.001. Ctrl: DMSO. (G, H) Representative images obtained by microscopy of SW872 cells treated with UDCA at a concentration of 400 μg/mL for 12 h, and representative Transmission electron microscope (TEM) images of SW872 cells treated with UDCA at concentrations of 200 μg/mL and 400 μg/mL for 12 h (G). The same applies to 93T449 cells (H). N: nucleus. (I, M) Reactive oxygen species (ROS) (DCFH-DA) levels measured in SW872 and 93T449 cells after treatment with UDCA (400 μg/mL). $n = 3$. Data are mean ± SD. $^{*}P$ <0.05, $^{**}P$ <0.01. (J, N) Flow cytometry of C11-BODIPY fluorescence in SW872 (J) and 93T449 (N) cells after treatment with UDCA for 6 h (400 μg/mL). (K, O) Malondialdehyde (MDA) levels in SW872 (K) and 93T449 (O) cells with UDCA treatment (400 μg/mL). $n = 3$. Data are mean ± SD. $^{**}P$ <0.01. (L, P) Cell viability of SW872 (L) and 93T449 (P) cells analyzed after treatment with UDCA alone or in combination with RSL3 (1 μM) and erastin (10 μM). $n = 3$. Data are mean ± SD. $^{***}P$ <0.001. Data were analyzed using two-tailed Student's *t*-tests.

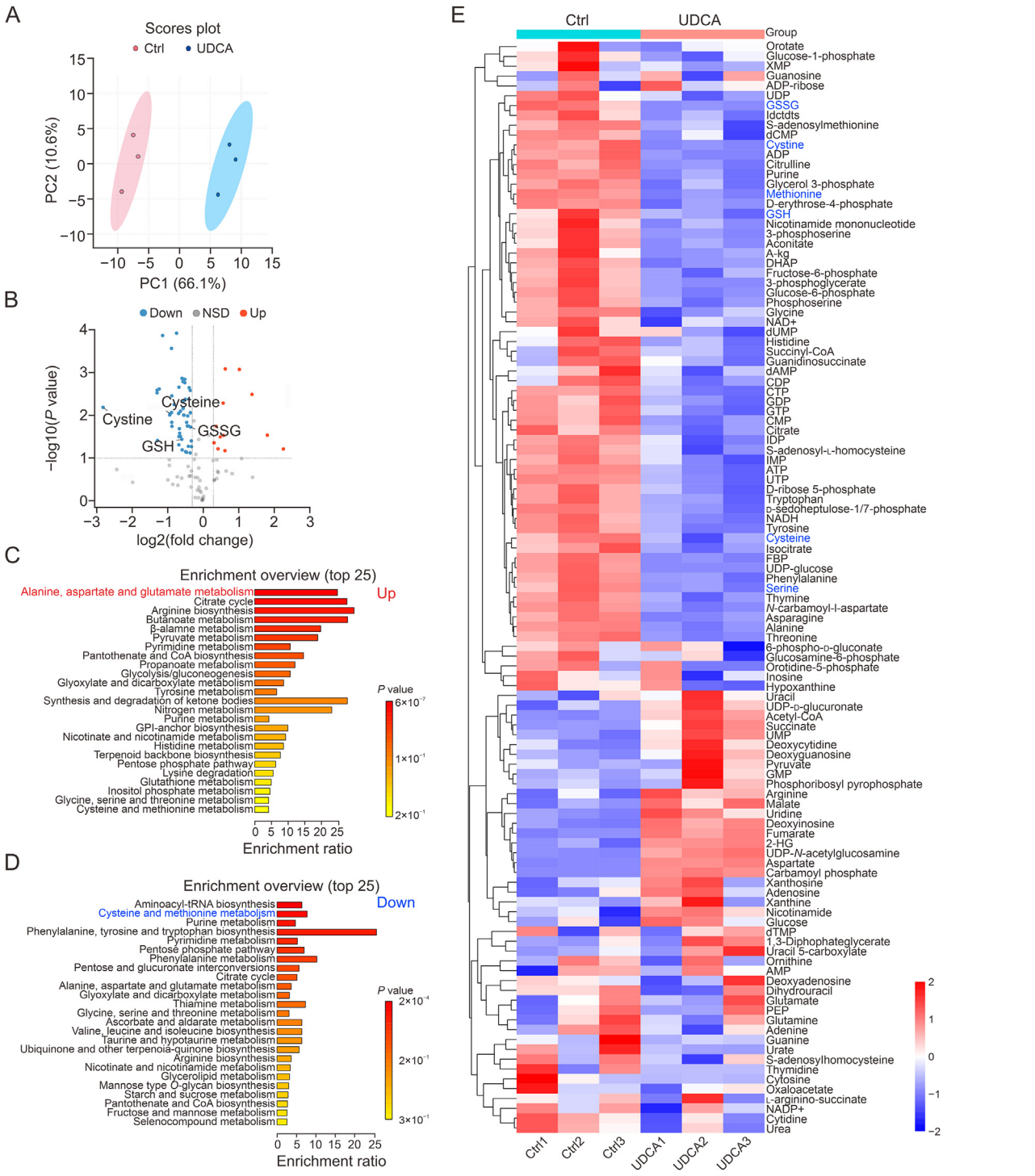

Fig. 3. Metabolome analysis of SW872 cells after treatment with UDCA. (A) Partial least squares discrimination analysis performed on the metabolome data. $n = 3$ per group. Ctrl: DMSO. (B) Volcano plots depict the relative abundance of differential metabolites in control and UDCA-treated cells where upregulated metabolites are labeled in red and downregulated ones in blue. $n = 3$ per group. NSD: no significant difference. (C, D). Kyoto Encyclopedia of Genes and Genomes (KEGG) functional enrichment analysis conducted on the differential metabolites in UDCA-treated SW872 cells. $n = 3$ per group. (E) A heatmap of the differential metabolites in UDCA-treated SW872 cells. $n = 3$ per group. Ctrl: control.

and 94T778) (Figs. 5A–D and S12A–D). Additionally, co-treatment with UDCA and cystine led to a significant increase in the level of GSH compared to the group treated with only UDCA in SW872 and 93T449 (Figs. 5E and F).

The above results indicate that cystine can rescue UDCA-mediated cell death, and previous study has also shown that albumin can chelate UDCA to reduce the concentration of free UDCA [28]. In this way, the presence of cystine and albumin in serum needs to be considered at both the cellular level and animal level. To imitate the physiological conditions under which cystine rescues UDCA-mediated cell death, we first cultured SW872 cells with different percentages of serum (0%, 5%, 10%, 20%, 30%, 40%, 50%, and 60%) in medium containing UDCA (400 μg/mL). It was found that UDCA significantly induced cell death when the serum

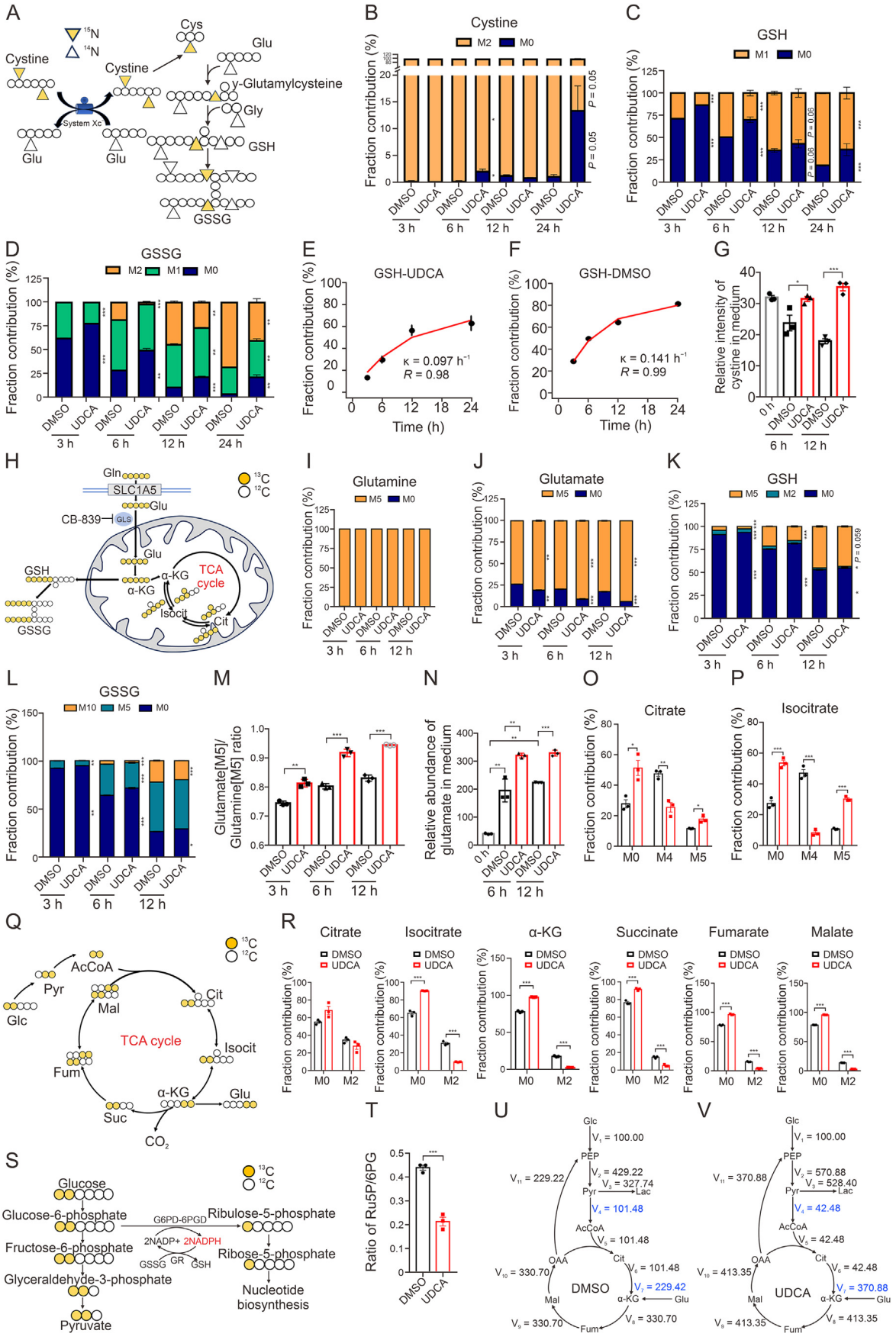
A
Cystine
Cys
Glu
Cystine
γ-Glutamylcysteine
Gly
GSH
System Xc
Glu
Glu
GSSG
B
Cystine
M2 M0
Fraction contribution (%)
P = 0.05
P = 0.05
DMSO UDCA DMSO UDCA DMSO UDCA DMSO UDCA
3 h 6 h 12 h 24 h
C
GSH
M1 M0
Fraction contribution (%)
P = 0.08
P = 0.08
D
GSSG
M2 M1 M0
Fraction contribution (%)
E
GSH-UDCA
κ = 0.097 h⁻¹
R = 0.98
Fraction contribution (%)
Time (h)
F
GSH-DMSO
κ = 0.141 h⁻¹
R = 0.99
Fraction contribution (%)
Time (h)
G
Relative intensity of cystine in medium
0 h DMSO UDCA DMSO UDCA
6 h 12 h
H
Gln
SLC1A5
Glu
CB-839
GLS
Glu
GSH
α-KG
α-KG
TCA cycle
Isocit
Cit
GSSG
13C
12C
I
Glutamine
M5 M0
Fraction contribution (%)
J
Glutamate
M5 M0
Fraction contribution (%)
K
GSH
M5 M2 M0
Fraction contribution (%)
P = 0.059
L
GSSG
M10 M5 M0
Fraction contribution (%)
M
Glutamate[M5]/ Glutamine[M5] ratio
N
Relative abundance of glutamate in medium
O
Citrate
Fraction contribution (%)
M0 M4 M5
P
Isocitrate
Fraction contribution (%)
M0 M4 M5
Q
13C
12C
AcCoA
Pyr
Glc
Mal
Cit
TCA cycle
Isocit
Fum
α-KG
Glu
Suc
CO2
R
Citrate
Isocitrate
α-KG
Succinate
Fumarate
Malate
DMSO
UDCA
Fraction contribution (%)
M0 M2
S
13C
12C
Glucose
Glucose-6-phosphate
G6PD-6PGD
Ribulose-5-phosphate
Fructose-6-phosphate
2NADP+ 2NADPH
GSSG GR GSH
Ribose-5-phosphate
Glyceraldehyde-3-phosphate
Nucleotide biosynthesis
Pyruvate
T
Ratio of Ru5P/6PG
DMSO UDCA
U
Glc
V1 = 100.00
PEP
V2 = 429.22
V3 = 327.74
Pyr
Lac
V4 = 101.48
AcCoA
V5 = 101.48
V11 = 229.22
OAA
Cit
V6 = 101.48
V10 = 330.70
DMSO
V7 = 229.42
Mal
α-KG
Glu
V9 = 330.70
Fum
V8 = 330.70
V
Glc
V1 = 100.00
PEP
V2 = 570.88
V3 = 528.40
V11 = 370.88
Pyr
Lac
V4 = 42.48
AcCoA
V5 = 42.48
OAA
Cit
V6 = 42.48
V10 = 413.35
UDCA
V7 = 370.88
Mal
α-KG
Glu
V9 = 413.35
Fum
V8 = 413.35

concentration was less than 30%. However, when serum concentrations were between 40% and 60%, UDCA could no longer mediate significant cell death (Figs. 5G and S12E). Second, to exclude the possibility that albumin's adsorption of UDCA blocked its mediated cell death, we analyzed whether dialyzed FBS without cystine could block UDCA-mediated cell death. We found that the cell viability in medium containing 30% FBS was significantly higher than in medium containing only 10% FBS after treatment with UDCA but not in dialyzed FBS (Figs. 5H and S12F). Thirdly, to further verify the effect of increasing cystine on rescuing UDCA-mediated cell death based on an increasing percentage of sera in the medium, and to verify that the same mechanism was used when the UDCA concentration decreased, we performed cystine rescue assays in the medium containing dialyzed serum. The results showed that additional cystine in medium containing dialyzed serum rescued UDCA mediated cell death (Fig. 5I).

Because UDCA-induced mitochondrial abnormalities may disrupt the balance of mitochondrial oxidative phosphorylation, we examined mitochondrial activity in cells treated with UDCA. We observed a significant inhibition of maximal respiratory rate, spare respiratory capacity, ATP production, and non-mitochondrial respiration measured as OCR upon UDCA treatment. However, this inhibition was rescued by cystine in SW872 cells (Figs. 5J and S13A). To further validate these findings *in vivo*, we initially assessed the toxicity of UDCA in mice. The results demonstrated that at a dose of 50 mg/kg/day, UDCA had no significant effects on blood routine examination, hepatic and renal function or body weight; however, at a dose of 250 mg/kg day there was a significant decrease in body weight (Fig. S14). Additionally, to evaluate the effect of UDCA with or without cystine on tumor growth *in vivo*, we compared their efficacy using a xenograft model where SW872 cells were subcutaneously injected into nude mice. Our results showed that while UDCA significantly retarded tumor growth alone (Fig. 5K), cystine partially rescued xenograft tumor growth (Figs. 5L and S15A).

As mentioned earlier, exposure to UDCA significantly increased the glutamate-to-glutamine ratio, indicating that UDCA promoted glutaminase activity. High levels of extracellular and intracellular glutamate inhibit the xCT system in cells, leading to impaired cystine uptake, reduced GSH synthesis, and increased ROS [29,30]. Glutaminase (GLS1 and GLS2) catalyzes the conversion of glutamine to glutamate. Additionally, P53 can activate GLS2 to upregulate glycolysis instead of oxidative phosphorylation, resulting in ferroptosis [31]. We further investigated the combination of UDCA and a glutaminase inhibitor for regulating cell death. Therefore, we performed CCK-8 assays, lipid peroxidation (MDA) assays, and Seahorse assays to assess the synergy between UDCA and CB-839 (telaglenastat), a glutaminase 1 inhibitor (50 nM *in vitro*; 250 mg/kg daily, *in vivo*), in liposarcoma cells. The results showed that exposure to UDCA combined with CB-839 treatment sensitized both SW872 and 93T449 cells to UDCA-induced cell death (Figs. 5M–P) and increased MDA levels (Figs. 5Q and R). However, the OCR results showed no significant difference between UDCA alone and UDCA combined with CB-839 (Figs. 5S and S13B). This indicates that increased glutamate does not enter the oxidation pathway of the tricarboxylic acid cycle (TCA) cycle to produce energy after stimulation with UDCA. The function of combining UDCA with CB-839 has also been verified *in vivo* (Figs. 5T and U and S15B). Taken together, the levels of glutamate in cancer cells are not contributed to mitochondrial oxidative phosphorylation upon UDCA treatment.

3.5. UDCA binds to SLC7A11 as an exchange factor of cystine

Previous reports have shown that SLC7A11-mediated cystine uptake regulates not only GSH synthesis but also the expression of GPX4 [32]. Our previous results suggested that UDCA stimulation led to the downregulation of intracellular cystine and GSH. Therefore, we first explored whether UDCA regulates the expression of SLC7A11. Interestingly, we observed that both UDCA alone and in combination with cystine downregulated GPX4 rather than SLC7A11 (Figs. 6A and S16), suggesting that the function of UDCA in inhibiting cystine transport and *de novo* synthesis of GSH was dispensable at the protein level of SLC7A11.

As mentioned above, UDCA inhibits intracellular GSH synthesis but not through downregulation of SLC7A11. Therefore, we wondered if UDCA could bind to SLC7A11 to prevent cystine binding or transport. Next, we investigated whether UDCA bound to SLC7A11 to hinder cystine uptake. The results from a precipitation-LC-MS/MS assay showed that the amount of UDCA pulled down by SLC7A11 in both the group pretreated with cystine plus post-treated with UDCA and the group co-treated with UDCA-cystine was significantly lower than the amount pulled down by the group treated only with UDCA (Fig. 6B). Furthermore, the amount of cystine pulled down by SLC7A11 in both the group pretreated with UDCA plus post-treated with cystine and by the group co-treated with UDCA-cystine was significantly lower than the amount pulled down by the cystine treatment group (Fig. 6C).

Therefore, we further investigated whether UDCA is transported into cells through SLC7A11. Firstly, we employed a molecular modeling approach and performed docking using Schrodinger-2018 software [33]. In our model, the amino acid residues I64, K67, L144, R148, E162, I165, K166, S300, N301, L385 and D386 formed a pocket for binding UDCA or cystine. Among them, I64, K67, R148, E162, and N301 were involved in hydrogen bonding with UDCA (Fig. 6D). To further confirm the binding of UDCA to SLC7A11

Fig. 4. Stable isotope tracing of SW872 cells after treatment with UDCA. (A) The schematic illustrates the incorporation of ^{15}N (yellow triangle) from cystine into the glutathione (GSH) synthesis pathway. (B) The ratio of intracellular labeled cystine (M2) measured at 3, 6, 12, and 24 h after treatment with UDCA or DMSO in medium containing [$^{15}N_2$]-cystine. $n = 3$. Data are mean ± SEM. $^{*}P$ <0.05. (C, D) The labeled and unlabeled GSH and GSSG levels in SW872 cells cultured in the medium containing [$^{15}N_2$]-cystine was measured when treated with UDCA and DMSO for 3, 6, 12, and 24 h. $n = 3$. Data are mean ± SEM. $^{**}P$ <0.01, $^{***}P$ <0.001. (E, F) GSH levels used to calculate the labeling rate (n =3 biological replicates in each time point) in the UDCA group (E) and control group (F); Black dots represent the median labeling extent, while whiskers represent ± SEM. (G) Relative intensity of cystine in medium determined after culturing SW872 cells with UDCA and DMSO for 6 and 12 h. $^{*}P$ <0.05, $^{***}P$ <0.001. (H) Schematic of ^{13}C (yellow cycle) incorporation of glutamine into the GSH synthesis pathway and tricarboxylic acid (TCA) cycle by [$^{13}C_5$]-Glutamine. (I–N) The labeled and unlabeled glutamine (I), glutamate (J), GSH (K), and GSSG (L) levels in SW872 cells cultured in the medium containing [$^{13}C_5$]-glutamine was measured when treated with UDCA and DMSO for 3, 6, and 12h. $n = 3$. Data are mean ± SEM. $^{*}P$ <0.05; $^{**}P$ <0.01; $^{***}P$ <0.001. The ratio of intracellular labeled glutamate [M5] to glutamine [M5] measured at 3, 6, and 12 h after treatment with UDCA or DMSO in medium containing [$^{13}C_5$]-glutamine. $n = 3$. Data are mean ± SEM. $^{**}P$ <0.01, $^{***}P$ <0.001 (M). Relative intensity of glutamate in medium after culturing SW872 cells with UDCA and DMSO for 6 and 12 h (N). The labeled and unlabeled citrate (O) and isocitrate (P) level in SW872 cells treated with UDCA and DMSO, cultured in medium containing [$^{13}C_5$]-glutamine. $n = 3$. Data are mean ± SEM. $^{*}P$ <0.05; $^{**}P$ <0.01; $^{***}P$ <0.001. (Q) Schematic of [$^{13}C_2$] (yellow cycle) incorporation from glucose into the TCA cycle. (R) Labeled and unlabeled metabolites level in SW872 cells treated with UDCA and DMSO, cultured in medium containing [$^{13}C_2$]-glucose. $n = 3$. Data are mean ± SEM. $^{***}P$ <0.001. (S) Schematic of [$^{13}C_2$] (yellow cycle) incorporation from glucose to produce nicotinamide adenine dinucleotide phosphate hydrogen (NADPH). (T) Ratio of ribulose-5-phosphate (Ru5P)/lucose-6-phosphate (G6P). $n = 3$. Data are mean ± SEM. $^{***}P$ <0.001. (U, V) Glycolysis and TCA cycle fluxes. Arrow represents the direction of net relative fluxes; number represents net relative flux. We fixed the glucose intake flux at 100 (V_1) at steady state by INCA software. After the cells were treated with UDCA, the metabolic flux of glutamine entering the TCA cycle increased (V_7). Glu: glutamate; Cys: cysteine; α-KG: alpha-ketoglutarate; Cit: citrate; Isocit: isocitrate; Pyr: pyruvate; Glc: glucose; Fum: fumarate; PEP: phosphoenol pyruvate; AcCoA: acetyl-CoA; Mal: malate; Suc: succinate.

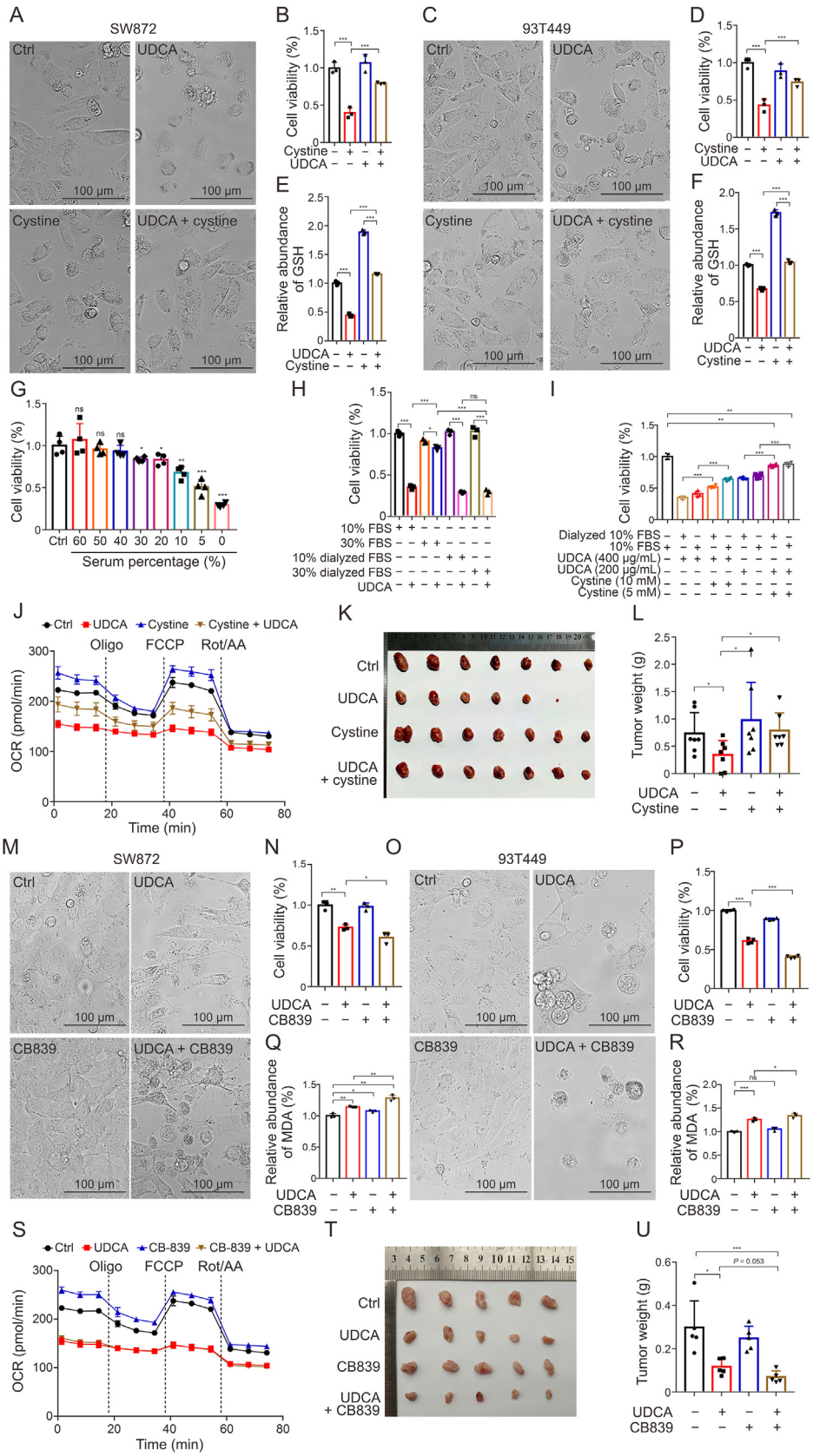

Fig. 5. Effect of cystine and CB839 on UDCA-mediated cell death. (A–D) Cell viability analyzed after treatment with UDCA (400 μg/mL) alone, cystine (10 mM) alone, and their combination for 12 h in SW872 (A, B) and 93T449 (C, D) cells. $n = 5$. Data are mean ± standard deviation (SD). $^{***}P$ <0.001. Ctrl: dimethyl sulfoxide (DMSO). (E, F) Glutathione (GSH) levels analyzed after treatment with UDCA (400 μg/mL) alone, cystine (10 mM) alone, and their combination for 12 h in SW872 (E) and 93T449 (F) cells. $n = 5$. Data are mean ± SD. $^{***}P$ <0.001. (G) Cell viability analysis of SW872 cells conducted after treatment with UDCA (400 μg/mL) in medium containing different percentages of serum. $n = 4$. Data are mean ± SD. $^{*}P$ <0.05, $^{**}P$ <0.01, $^{***}P$ <0.001; ns: not significant. (H) Cell viability analysis of SW872 cells conducted after treatment with UDCA (400 μg/mL) in medium with fetal bovine

or its complex formation, a biotin-labeled molecule called UDCA-EA-Biotin was synthesized by attaching an ethyleneamine biotin group to the carboxyl terminus of UDCA (Fig. 6E). Co-immunoprecipitation assays were performed to detect the interaction between UDCA and SLC7A11 (Figs. 6F and G). The colocalization of UDCA-EA-Biotin with SLC7A11 was observed in SW872 and 93T449 cells. Furthermore, lentiviruses carrying control vectors (wild type), SLC7A11 overexpression vectors (SLC7A11 OV) and SLC7A11 knockdown vectors (SLC7A11 KD) were used to establish stable cell lines expressing these constructs (Fig. 6H). Silencing of SLC7A11 impaired the uptake of UDCA. On the contrary, the transport of UDCA into cells was significantly enhanced when SLC7A11 was overexpressed (Figs. 6I and J). Moreover, the effect of UDCA on cell death in these three cell lines was examined (Fig. 6K). After treatment with UDCA (400 μg/mL) for 24 h, SLC711 knockdown cells showed resistance to UDCA-mediated cell death. However, SLC711 over expressing cells exhibited sensitivity to UDCA-mediated cell death, supporting our hypothesis that UDCA was transported into cells through SLC711.

To determine whether the reduction of intracellular transport of cystine is caused by UDCA transport, we first detected intracellular and extracellular levels of UDCA, glutamate, and cystine after UDCA treatment (Figs. 6L–N). The results showed that as intracellular UDCA increased, intracellular cystine and extracellular UDCA decreased. This confirmed once again that the inhibition of intracellular cystine transport was accompanied by the transport of UDCA into cells. Next, when the glutaminase inhibitor CB-839 was combined with UDCA, both intracellular and extracellular levels of glutamate significantly decreased while intracellular UDCA also decreased (Figs. 6O–R). Furthermore, compared to using only UDCA alone, the combination of UDCA and CB-839 significantly reduced intracellular cystine levels (Figs. 6S and T). These results indicated that SLC7A11 bound to and transported UDCA into cells in the presence of glutamate while preventing cystine from being transported into cells through SLC7A11. At the same time, these results also explain why there is a decrease in serum levels of UDCA in RLPS patients. Based on these findings, we hypothesized that the abundance of SLC7A11 is related to sensitivity towards cell death induced by UDCA treatment. We selected human umbilical vein endothelial cells (HUVECs), human bronchial epithelial cells (Beas-2B), human embryonic kidney cells (293T), human dedifferentiated liposarcoma cells (SW872), human well-differentiated liposarcoma cells (93T449, 94T778), and human primary retroperitoneal dedifferentiated liposarcoma cells (XMU-RC-1, XMU-RC-2) to examine expression of SLC7A11. Notably, SLC7A11 was highly expressed in RLPS. By investigating the other six cell lines treated with UDCA (400 μg/mL) for 24 h, we observed that the upregulation of SLC7A11 expression corresponded to increased sensitivity of the cells to UDCA-induced cell death (Fig. S17).

3.6. UDCA sensitizes cells to MDM2 inhibitor-mediated antitumor therapy in multiple types of tumor cells

Given that UDCA binds to SLC7A11 to suppress cystine uptake and amplification of the *mdm2* is a diagnostic marker for RLPS, we further examined the protein levels of SLC7A11, MDM2, and CD36 (an adipose tissue biomarker). Immunohistochemistry (IHC) assays showed significant downregulation of CD36 in 50 RLPS tissues compared with normal adipose tissues, while both SLC7A11 and MDM2 were upregulated. Western blot assays of 17 human RLPS tissues also yielded similar results (Figs. 7A and B). The correlation between SLC7A11 and MDM2 exhibited good linearity (R^2 = 0.618) (Fig. S18). Moreover, we also measured the intermediate metabolites in methionine and cystine metabolism using LC-MS/MS in clinical tissues and found that cystine levels were significantly higher in liposarcoma tissue than in adjacent adipose tissue, while serine and methionine levels were significantly lower (Figs. S19). This indicated that in liposarcoma tissue, exogenous and endogenous cystine were required for the synthesis of cysteine. Interestingly, we found that both serine and methionine were significantly downregulated after UDCA treatment (Figs. 3 and S9). Moreover, MDM2-mediated serine metabolism was required for liposarcoma growth through a P53-independent metabolic pathway, which explained the poor clinical efficacy of inhibitors targeting the MDM2-P53 interaction [34]. We also found that UDCA mediated more cell death when *MDM2* was knocked down (Fig. S20). Several drugs have been developed to target MDM2. However, many preclinical studies showed negative effects of these drugs on lymphoid organs and the gastrointestinal tract. We further performed a pan-cancer analysis of MDM2 and SLC7A11. Among the selected types of tumors, MDM2 and SLC7A11 levels in tumors were significantly higher than those in adjacent tissues (Figs. 7C and D). As the key molecule of the MDM2-P53 signaling axis, MDM2 is one of the most important targets for screening antitumor drugs, such as nutlin-3a, RG7112, and SAR405838. Of note, nutlin-3a is a potent inhibitor of MDM2 that inhibits MDM2-P53 interactions and stabilizes the P53 protein, whereas RG7112 is the first clinically available, orally available, blood-brain barrier permeable, and potent MDM2-P53 inhibitor. Herein, we further asked whether the combination of UDCA and an MDM2 inhibitor could provide a promising effect for liposarcomas or other types of tumors. We performed a cell viability assay, and surprisingly, the synergistic effect of UDCA combined with an MDM2 inhibitor, either nutlin-3a or RG7112, showed that the combined strategy promoted severe cell death compared to MDM2 inhibitor alone (Figs. 7E–L).

We know that a lower concentration of UDCA is preferred for the clinical application of anti-cancer therapy. In Figs. 2A and B, we observed that UDCA at concentrations of 50 μg/mL and 25 μg/mL can inhibit the proliferation of liposarcoma cell lines. To determine whether these concentrations can promote an anti-cancer effect, cytotoxicity tests were performed using liposarcoma (SW872), colorectal cancer (HCT116), and cholangiocarcinoma (QBC939) cell lines. The results showed that UDCA at a concentration of 50 μg/mL can enhance the anti-cancer effects of CB-839, Nutlin3a, Abemaciclib (a clinically used chemotherapeutic drug for retroperitoneal sarcoma targeting CDK4), and RSL3 (Fig. S21). Additionally, UDCA at a concentration of 25 μg/mL for 24 h can enhance the anti-cancer effects of Nutlin3a and Abemaciclib.

serum (FBS) and dialyzed FBS. $n = 3$. Data are mean ± SD. $^{*}P$ <0.05, $^{***}P$ <0.001; ns: not significant. (I) Cell viability analysis of SW872 cells conducted after treatment with different concentrations of UDCA and cystine in medium supplemented with FBS or dialyzed FBS. $n = 4$. Data are mean ± SD. $^{**}P$ <0.01, $^{***}P$ <0.001. (J) Oxygen consumption rates (OCR) investigated after treatment with UDCA (400 μg/mL) and cystine (10 mM) alone and in combination for 12 h in SW872 and 93T449 cells. $n = 3$. Data are mean ±SEM. (K, L) Analysis of the effects of UDCA (250 mg/kg per day) and cystine (1 mmol/kg per day) alone and in combination on the subcutaneous tumorigenic ability of SW872 cells. n=7. Data are mean ± SD. *p<0.05. (M–P) Cell viability analyzed after treatment with UDCA (400 μg/mL) and CB839 (50 nM) alone or in combination for 12 h in SW872 (M, N) and 93T449 (O, P) cells. n = 5. Data are mean ± SD. $^{*}P$ <0.05, $^{**}P$<0.01, $^{***}P$<0.0001. (Q, R) Malondialdehyde (MDA) levels tested after treatment with UDCA (400 μg/mL) and CB839 (50 nM) alone or jointly for 12 h in SW872 (Q) and 93T449 (R) cells. $n = 3$. Data are mean ± SD. $^{*}P$ <0.05, $^{**}P$ <0.01, $^{***}P$ <0.001; ns: not significant. (S) The OCR investigated after treatment with UDCA (400 μg/mL) and CB839 (50 nM) alone and jointly for 12 h in SW872 cells. $n = 3$. Data are mean ± SEM. (T, U) Analysis of the effects of UDCA (250 mg/kg per day) and CB839 (200 mg/kg per day) alone and in combination on the subcutaneous tumorigenic ability of SW872 cells. n=5. Data are mean ± SD. $^{**}P$ <0.01, $^{***}P$ <0.001. Oligo: oligomycin; FCCP: carbonyl cyanide 4-(trifluoromethoxy)phenylhydrazone; Rot/AA: rotenone/antimycin.

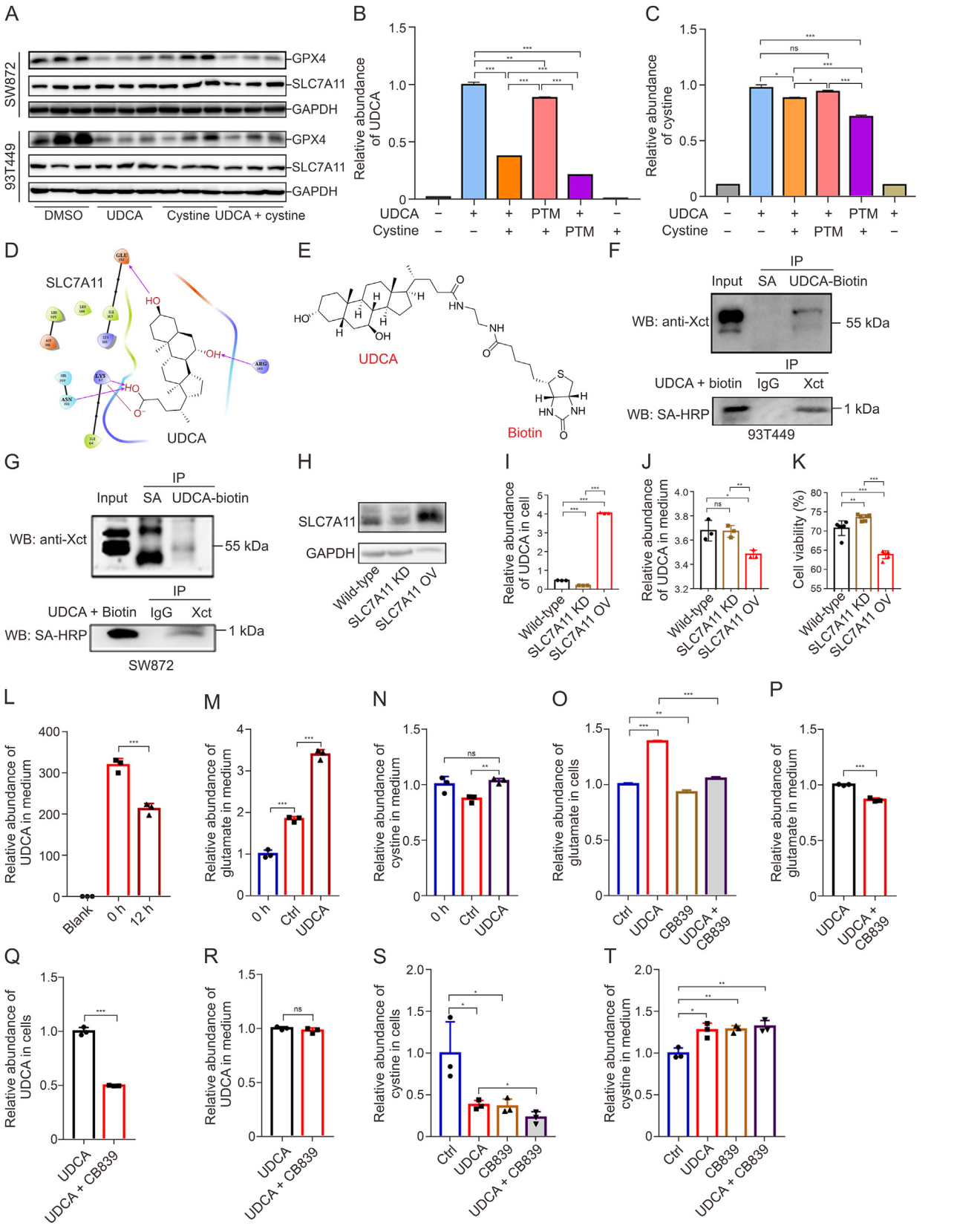

Fig. 6. Analysis of UDCA binding and transportation based on SLC7A11. (A) Western blot analysis conducted to examine GPX4 and SLC7A11 cells after treatment with UDCA and cystine alone and jointly in SW872 cells for 12 h. $n = 3$. Data are mean ± standard deviation (SD). (B, C) Binding inhibition analysis of UDCA (B) and cystine (C) to SLC7A11. $n = 3$. Data are mean ± SEM. $^{*}P$ <0.05, $^{**}P$ <0.01, $^{***}P$ <0.001; ns: not significant. (D) Molecular modeling and docking analysis performed by Schrodinger 2018 software, with wild-type SLC7A11 and the predicted binding sites. (E) Chemical structure of UDCA and ethylenediamine biotin (EA-Biotin) conjugated compound (UDCA-Biotin). (F, G) Co-immunoprecipitation analysis of the interaction between UDCA-Biotin and SLC7A11 in 93T449 (F) and SW872 (G) cells. (H) Western blot analysis of SLC7A11 wild-type (empty vector), *SLC7A11* knockdown (SLC7A11 KD) and *SLC7A11* overexpression (SLC7A11 OV) SW872 cell lines. (I, J) Relative abundance of UDCA in cell (I) and culture medium (J) after treating with UDCA

4. Discussions

Our study found that UDCA has a dual effect on promoting and suppressing liposarcoma development depending on the dosage. Further studies are needed to determine the mechanism by which UDCA promotes RLPS. This study mainly focused on cancer suppression, providing a theoretical basis for UDCA-assisted cancer treatment through targeting SLC7A11 and impairing GSH synthesis, eventually leading to uncleared ROS, mitochondrial oxidative damage, and cell death. Our findings differ from previous reports that suggest UDCA can up-regulate cell ROS levels and lead to apoptosis [8]. Here we have shown that ROS accumulation may be due to impaired GSH synthesis, resulting in an inability to effectively eliminate ROS. This provides a new perspective and mechanism for UDCA-mediated cell death. The submicroscopic structure of liposarcoma cells treated with UDCA differed from classic apoptosis, necrosis, autophagy, pyroptosis, and ferroptosis; although some altered metabolite and protein levels and pathways were closely associated with ferroptosis and apoptosis (Figs. 2G and H, 3, S5, and S8–S10). We hypothesized that the observed phenomenon may be attributed to the activation of multiple types of cell death caused by decreased GSH and increased ROS. The detailed mechanism may be related to the concentrations and exposure times of UDCA, cystine, glutamate, serine, and methionine, as well as the expression abundance of SLC7A11, P53, GLS2 or other unidentified proteins.

As a group of adipocytic tumors originating from mesenchymal cells [35], both DDLPSs and WDLPSs are different from adipocytes. Recent progress in the last decade using targeted sequencing, RNA sequencing, whole-exome sequencing or whole-genome sequencing have identified amplifications of MDM2, CDK4, HMGA2, TSPAN31, CPM, YEATS4, FRS2 and PTPRB in RDDLPS and RWDLPS [36]. Multi-omics joint analysis of RWDLPS/RDDLPS has revealed the metabolic profile of retroperitoneal liposarcoma [37]. Despite these above enhancing our understanding of the genetic basis driving the development of RWDLPS and RDDLPS, however, the characteristics of RLPS patient's serum remain unclear. In this study, we identified a total of 756 lipids using with reference standards and LC/MS fragmentation by searching against our home-made database (Figs. 1 and S1, and Table S2). Intriguingly, we found that UDCA was one of the most significantly decreased metabolites in the sera of patients with RLPS compared to healthy controls (Fig. 1C). UDCA is a secondary bile acid in the body that can be transformed from (cheno) deoxycholic acid by intestinal bacteria. It plays in a key role in lipid metabolism, and exhibits both pro- and anti-apoptotic properties, depending on the cell type [8]. Absolute quantification of UDCA in a larger cohort of RLPS patients showed a decreased concentration of UDCA in the sera compared to healthy controls (Fig. 1D). Interestingly, we found that the concentration of UDCA in postoperative patients' sera was significantly higher than in preoperative retroperitoneal DDLPS samples, which was also verified in a mouse model (Figs. 1E and F). Overall, our findings suggest for the first time a significant decrease of UDCA levels in serum among patients with RLPS. The decline of UDCA indicates that it may serve as a potential diagnostic marker for retroperitoneal liposarcoma; however, further studies are needed to determine its specificity and sensitivity. Additionally, what could be causing this decline? Do gut flora or sarcoma tissue play regulatory roles? Does UDCA play any role in the occurrence and development of retroperitoneal sarcoma, immune regulation, chemotherapy resistance, etc.? Our study provides a foundation for further research on the function and mechanism of UDCA in RLPS.

Liposarcoma, a rare type of cancer, tends to grow rapidly to a large size and appears to be insensitive to chemotherapy [38]. Anthracycline-based therapy and targeted therapy targeting MDM2 and CDK4 have been used for the treatment of liposarcoma [39]. However, there remains a lack of effective treatments for advanced and metastatic liposarcomas. Surgery is still the most efficient approach in treating liposarcoma; however, the relapse rate after surgery exceeds 50%. Therefore, alternative approaches to surgery and potential synergistic strategies are needed. We discovered that UDCA impairs GSH de novo synthesis in cells, leading to intracellular ROS accumulation and oxidative damage. This observation is crucial for cancer treatment since UDCA can assist with therapeutic strategies that generate high levels of ROS such as hyperthermic chemotherapy, photothermal and photodynamic therapy, hyperthermia radiotherapy, as well as various chemotherapeutic drugs including platinum compounds, gemcitabine, MMD2 inhibitors (rg7112, nutlin3a), and l-Ascorbic acid. The anticancer effects could be significantly enhanced if UDCA were combined with these chemotherapeutic drugs. In this study, we verified that UDCA can enhance the anti-cancer effects of the ferroptosis inducers (erastin and RSL3) (Figs. 2L and P, and S7), the MDM2 inhibitor (Nutlin 3a, and RG7112) (Figs. 2E–L), the CDK4 inhibitor (abemaciclib) (Fig. S21), and the glutaminase inhibitor (CB839) (Figs. 5M–R). Ferroptosis is a non-apoptotic form of cell death that has not been previously described in liposarcoma. It can potentially be utilized to eliminate cancer cells by inducing metabolic imbalance-induced cell death. The balance between amino acid and lipid metabolism plays a critical role in ferroptosis regulation. There are five main pathways involved in governing ferroptosis: GSH/GPX4 pathway, FSP1/DHODH/CoQ10 pathway, GCH1/BH4 pathway, iron metabolism pathway, and lipid metabolism pathway [40]. Erastin inhibits voltage-dependent anion channels (VDAC2/VDAC3) and accelerates oxidation, leading to endogenous ROS accumulation which causes mitochondrial damage through NADH-dependent ROS production [41]. RSL3 is an inhibitor of GPX4, independent of VDAC, which binds and inactivates GPX4, resulting in GPX4 being unable to use GSH to clear ROS [41]. Glutamine can also generate aspartate, which serves as the carbon source for pyrimidine biosynthesis, and glutathione to maintain redox balance. Depletion of pyrimidines and increased ROS were observed with glutaminase inhibitors [42]. Telaglenastat (CB-839) is a selective, reversible, and orally active glutaminase inhibitor that induces apoptosis through ROS [43]. WDLPS and DDLPS account for 60 % of all liposarcomas, reflecting the heterogeneity of this type of sarcoma. Genetically, both types of liposarcomas are characterized by amplification of MDM2 and CDK4 genes, indicating an important molecular event with diagnostic and therapeutic relevance [38].

The tumor suppressor protein p53 is a redox-active transcription factor that organizes and directs cellular responses in the face of various stresses leading to genomic instability. Reactive oxygen species (ROS), generated by cells as products or by-products, can function either as signaling molecules or as cellular toxicants. Cellular generation of ROS is central to redox signaling. Recent studies have revealed that each cellular concentration and distribution of p53 has

in wild type, SLC7A11 KD and SLC7A11 OV cell lines. $n = 3$. Data are mean ± SD. $^{*}P$ <0.05, $^{**}P$ <0.01, $^{***}P$ <0.001; ns: not significant. (K) Cell viability of wild type, SLC7A11 KD and SLC7A11 OV cell lines assessed after treatment with UDCA for 12 h. $n = 5$. Data are mean ± SEM. $^{*}P$ <0.05, $^{***}P$ <0.001. (L–N) Relative abundances of UDCA (L), glutamate (M), and cystine (N) in the culture medium. $n = 3$. Data are mean ± SEM. $^{**}P$ <0.01, $^{***}P$ <0.001; ns: not significant. (O–T) Relative abundances of glutamate (O, P), UDCA (Q, R), and cystine (S, T) in cells and medium when treated with UDCA and CB839 (1 μM). Data are mean ± SEM. $^{*}P$ <0.05, $^{**}P$ <0.01, $^{***}P$ <0.001; ns: not significant. Ctrl: DMSO; PTM: pre-treatment; SA: streptavidin; Xct: Xct antibody.

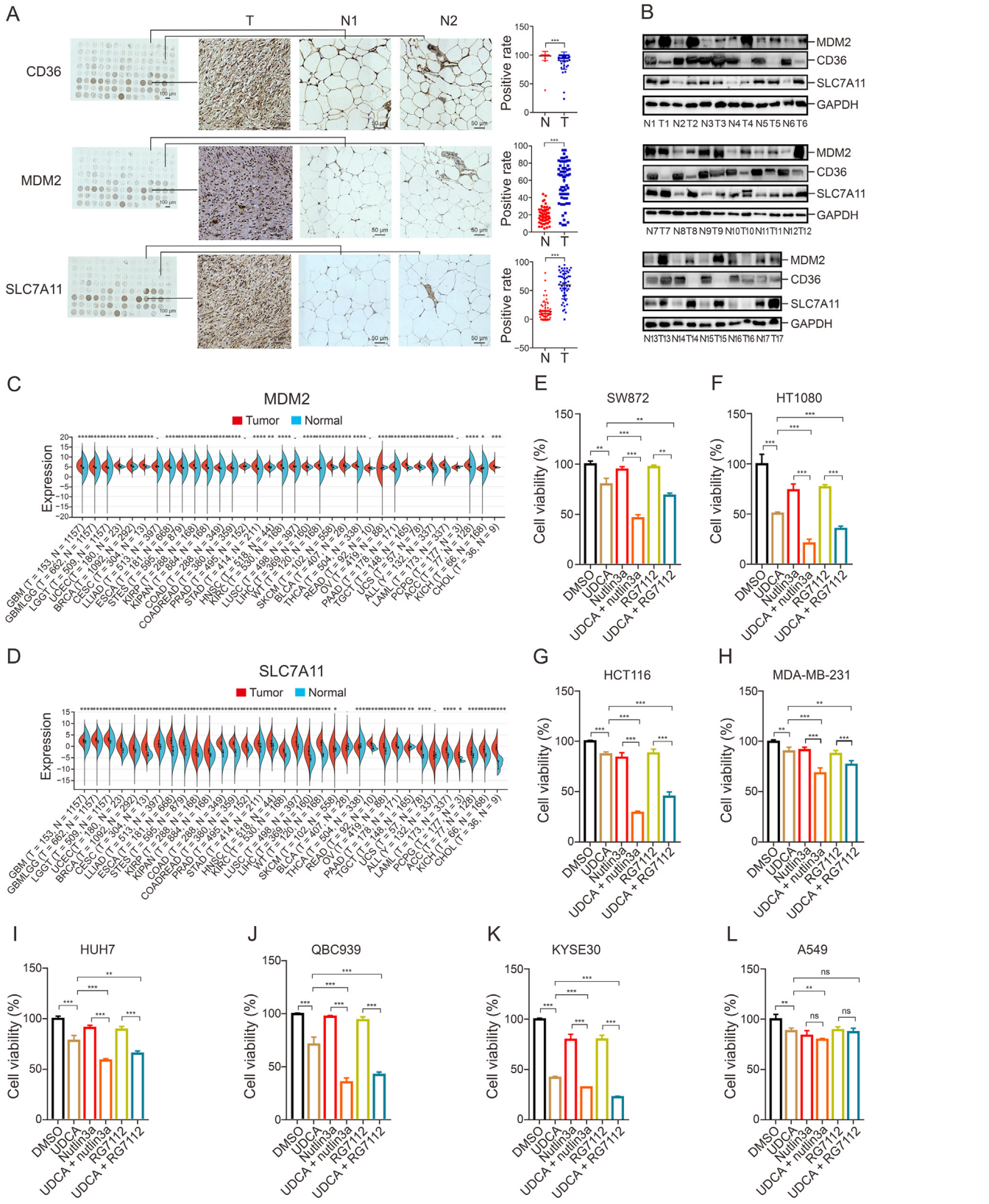

Fig. 7. Expression of SLC7A11 in clinical tissue samples of retroperitoneal liposarcoma (RLPS) and UDCA sensitizes cells to reactive oxygen species (ROS) induced inhibitor-mediated antitumor therapy in multiple types of tumor cells. (A) Immunohistochemistry (IHC) staining of RLPS tissue and adjacent adipose tissue microarrays with the indicated antibodies. $n = 50$. Data are mean ± standard deviation (SD). $^{***}P < 0.001$. (B) MDM2, CD36, and SLC7A11 in RLPS and adjacent adipose tissue lysates from patients suffering from retroperitoneal dedifferentiated liposarcoma and well-differentiated liposarcoma detected by Western blot assay with the indicated antibodies. $n = 17$. (C, D) Pan-cancer analysis of MDM2 (C) and SLC7A11 (D) (http://www.sangerbox.com/home.html). (E–L) Cell viability analyzed after treatment with UDCA (400 μg/mL), nutlin3a (10 μM), and RG7112 (5 μM) either alone or in combination for 24 h in DDLPS (SW872) (E), fibrosarcoma (HT1080) (F), colorectal cancer (HCT116) (G), breast cancer (MDA-MB-231) (H), liver cancer (HUH7) (I),

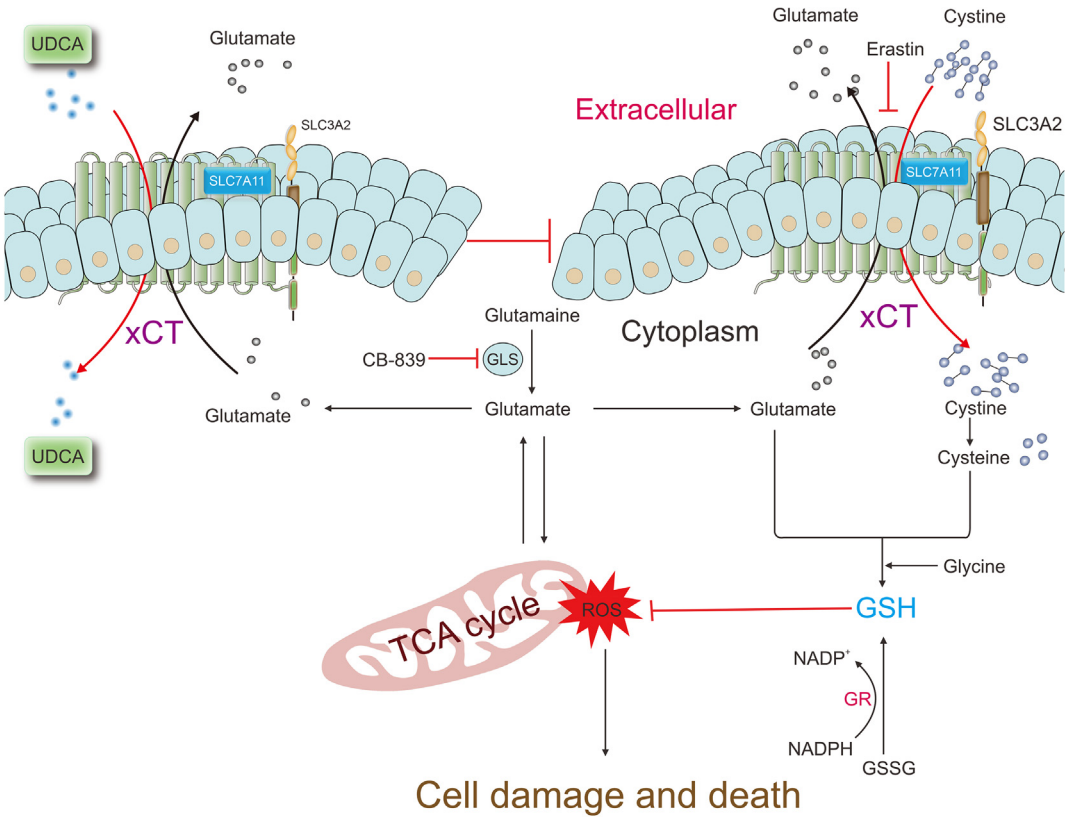

Fig. 8. Schematic model for the mechanism UDCA suppresses SLC7A11-based cystine uptake and impairs glutathione (GSH) *de novo* synthesis. UDCA inhibits the intracellular transport of cystine, leading to decreased levels of intracellular cystine, cysteine, and GSH. This subsequently results in mitochondrial damage and disorder in the tricarboxylic acid cycle (TCA) cycle.

a distinct cellular function and that ROS act as both an upstream signal that triggers p53 activation and a downstream factor that mediates apoptosis [44]. RG7112 is a potent, selective, first clinical, orally active and blood-brain barrier crossed MDM2-p53 inhibitor [45]. Nutlin-3a (Rebemadlin), is a potent murine double minute (MDM2) inhibitor. RG7112 and Nutlin-3a can inhibit MDM2-p53 interactions and stabilizes the p53 protein, and induces cell autophagy and apoptosis [46]. Abemaciclib (LY2835219) is a selective CDK4/6 inhibitor. Abemaciclib considerably inhibited the growth of PC cells in a dose-dependent manner ($P < 0.01$) and caused significant apoptotic cell death through the suppression of CDK4/6-Cyclin D complex, ROS generation and depolarization of mitochondria membrane potential [47]. Cotargeting CDK4/6 and BRD4 Promotes Senescence and Ferroptosis Sensitivity in Cancer [48]. Thus, the exploration of methodologies for the reduction of drug concentrations and the development of combination strategies will constitute significant avenues of research in the future. Consequently, our study calls for further exploration of UDCA in combination with other drugs.

In addition to system Xct-mediated exogenous cystine transport into cells for cysteine production, cellular cysteine can also be synthesized from serine and methionine through the transsulfuration pathway [49], which is an alternative process for producing GSH to eliminate ROS. In clinical samples, we observed that the levels of cystine in liposarcoma tissue were significantly higher than those in adjacent adipose tissue, while the levels of serine and methionine were significantly lower (Figs. S19 A–C). This suggests that in liposarcoma tissue, the synthesis of cysteine requires not only a large substantial of exogenous cystine but also endogenous cysteine derived from serine and methionine via the transsulfuration pathway. Interestingly, we found that both serine and methionine were significantly downregulated after UDCA treatment (Figs. 3 and S8). Furthermore, MDM2-mediated serine metabolism was essential for liposarcoma growth through a P53-independent metabolic pathway mechanism. A previous study explained why inhibitors targeting MDM2-P53 interaction had poor clinical efficacy [34]. We also found that UDCA mediated more cell death when MDM2 was knocked down (Fig. S20). Additionally, clinical verification revealed a positive correlation between SLC7A11 and MDM2 in RLPS tissue. In the current study, the combination of UDCA with the MDM2 inhibitors RG7112 or nutlin-3a also demonstrated a more effective intervention in multiple types of tumors, including liposarcoma,

cholangiocarcinoma (QBC939) (J), esophageal cancer (KYSE30) (K), and lung cancer (A549) (L), cells. n=5. Data are mean ± SD. $^{**}P$ <0.01, $^{***}P$ <0.001; ns: not significant. CD36: fatty acid transporter, highly expressed in fat tissue; MDM2: nuclear-localized E3 ubiquitin ligase, a biomarker for retroperitoneal dedifferentiated and well-differentiated liposarcoma; T: retroperitoneal liposarcoma; N: adjacent normal adipose tissue; GBM: glioblastoma multiforme; GBMLGG: glioma; LGG: brain lower grade glioma; UCEC: uterine corpus endometrial carcinoma; BRCA: breast invasive carcinoma; CESC: cervical squamous cell carcinoma and endocervical adenocarcinoma; LUAD: lung adenocarcinoma; ESCA: esophageal carcinoma; STES: stomach and esophageal carcinoma; KIRP: kidney renal papillary cell carcinoma; KIPAN: pan-kidney cohort; COAD: colon adenocarcinoma; COADREAD: colon adenocarcinoma; PRAD: prostate adenocarcinoma; STAD: stomach adenocarcinoma; HNSC: head and neck squamous cell carcinoma; KIRC: kidney renal clear cell carcinoma; LUSC: lung squamous cell carcinoma; LIHC: liver hepatocellular carcinoma; WT: high-risk Wilms tumor; SKCM: skin cutaneous melanoma; BLCA: bladder urothelial carcinoma; THCA: thyroid carcinoma; READ: rectum adenocarcinoma; OV: ovarian serous cystadenocarcinoma; PAAD: pancreatic adenocarcinoma; TGCT: testicular germ cell tumors; UCS: uterine carcinosarcoma; ALL: acute lymphoblastic leukemia; LAML: acute myeloid leukemia; PCPG: pheochromocytoma and paraganglioma; ACC: adrenocortical carcinoma; KICH: kidney chromophobe; CHOL: cholangiocarcinoma.

fibrosarcoma, lung cancer, liver cancer, breast cancer, cholangiocarcinoma, and colorectal cancer (Figs. 7E–L and S21). These results indicate that UDCA enhances the pharmacological inhibition of the MDM2-P53 interaction. We found that SLC7A11 can act as a transporter for UDCA. RLPS cells with high expression of SLC7A11 have a high absorption capacity for UDCA (Fig. 6I). Moreover, RLPS often tends to form large sizes, which explains the decrease in UDCA levels in the serum of RLPS patients (Fig. 1). This hypothesis seems to contradict the notion that UDCA would induce liposarcoma cell death if it were absorbed by liposarcoma cells. However, our results showed that both UDCA and cystine compete to bind with SLC7A11 (Figs. 6B and C). High concentrations of cystine rescued UDCA-mediated cell death, leading to impaired GSH synthesis (Figs. 5A–L and S12). According to clinical studies, the normal physiological concentration of UDCA in sera ranges from 4.7 to 264 μg/L (0.016 μM–0.88 μM) [26], while the concentration of cystine is between 80 mg/L and 110 mg/L (0.33 mM–0.45 mM) [50]. These studies suggest that reducing cystine concentration in sera is necessary when using UDCA-based therapy since its concentration is almost a thousand times higher than that of UDCA under normal physiological conditions; thus making it difficult for UDCA to exhibit an antitumor effect at normal physiological concentrations alone requires controlling cystine levels in serum during tumor treatment utilizing UCDA therapy effectively even more so for patients with homocysteinemia may not be effective this regimen also indicates early administration or post-surgery use may yield better results combining other drugs lowering the concentration of UCDA coupling chemotherapy drugs at carboxyl end.

There are several limitations to the present study. First, due to retroperitoneal sarcoma being a rare malignancy sarcoma originating from mesenchymal tissue in the retroperitoneal space, which encompasses over 50 pathological types, it is only found that UDCA decreases in retroperitoneal differentiated liposarcoma and retroperitoneal well-differentiated liposarcoma in this study. However, further investigation is needed to determine if UDCA also decreases in other types of RPS. Second, there is a lack of clinical trial support for UDCA and UDCA-assisted anti-tumor treatment strategies with other drugs. More research is required to elucidate the mechanisms and side effects involved. Thirdly, the intracellular interaction mechanism of UDCA when transported into cells needs further exploration; for example, how does UDCA regulate glutamate metabolism? Fourthly, more regulatory mechanisms of UDCA in RLPS patients need to be researched further. Additionally, the specificity and accuracy of using UDCA as a diagnostic and prognostic marker for RLPS should be studied on larger cohorts.

5. Conclusions

In conclusion, we conducted a lipidomic analysis of serum from patients with RLPS and observed a significant decrease in UDCA levels followed by rebound after surgery. The functions and mechanisms of UDCA varied among different cancer cells depending on treatment duration, dose, and combinations with other drugs. Importantly, contrary to previous reports suggesting that UDCA upregulates P53 to induce apoptosis through ROS production, our study revealed that UDCA inhibited SLC7A11-mediated cystine transport into cells, resulting in impaired synthesis of GSH and increased sensitivity to ROS (Fig. 8). This study not only provides new insights into the mechanism and transporter of bile acids in tumors but also establishes a theoretical foundation for further research on anti-tumor strategies involving UDCA. These findings encourage us to investigate the relationship between tumorigenesis and other bile acids such as EDCA, which also exhibit a notable decrease in the serum of liposarcoma patients.

CRediT authorship contribution statement

Fu'an Xie: Writing – original draft, Methodology, Investigation, Formal analysis, Data curation. **Yujia Niu:** Investigation, Formal analysis, Data curation. **Xiaobing Chen:** Resources, Investigation. **Xu Kong:** Investigation, Formal analysis, Data curation. **Guangting Yan:** Investigation. **Aobo Zhuang:** Investigation. **Xi Li:** Writing – review & editing, Formal analysis. **Lanlan Lian:** Resources. **Dongmei Qin:** Investigation. **Quan Zhang:** Software, Methodology, Formal analysis. **Ruyi Zhang:** Investigation. **Kunrong Yang:** Resources. **Kun Chen:** Resources. **Mengmeng Xiao:** Resources, Resources. **Chunkang Yang:** Resources. **Ting Wu:** Project administration, Data curation. **Ye Shen:** Investigation. **Chundong Yu:** Supervision, Project administration, Conceptualization. **Chenghua Luo:** Supervision, Resources, Conceptualization. **Shu-Hai Lin:** Supervision, Funding acquisition, Conceptualization. **Wengang Li:** Supervision, Funding acquisition, Conceptualization.

Data availability

All data associated with this study are presented in the paper or the supplemental materials. Materials will be shared with the scientific community by contacting Wengang Li. The mass spectrometry data for metabolomics have been deposited in MetaboLights (https://www.ebi.ac.uk/metabolights/), which is accessible using the identifiers MTBLS5260 for serum lipidomics, MTBLS5290 for absolute quantification of serum metabolites, and MTBLS5306 for cellular metabolomics and stable isotope tracing.

Declaration of competing interest

The authors declare that there are no conflicts of interest.

Acknowledgments

We thank Haiping Zheng at the Central laboratory, School of Medicine, Xiamen University for providing scientific and technical support. This work was supported by grants from the National Natural Science Foundation of China (Grant NOs.: 82272935, 91957120 and 21974114), the Postdoctoral Fellowship Program of CPSF (Program No.: GZC20240901), the Xiamen Medical Industry Combined Guidance Project (Project No.: 3502Z20244ZD2022), the Scientific Research Foundation for Advanced Talents, Xiang'an Hospital of Xiamen University (Grant No.: PM20180917008), the Fundamental Research Funds for the Central Universities (Grant No.: 20720210001) and Major Science and Technology Special Project of Fujian Province (Project No.: 2022YZ036012), Joint Laboratory of School of Medicine, Xiamen University-Shanghai Jiangxia Blood Technology Co., Ltd. (Grant No.: XDHT2020010C), and Joint Research Center of School of Medicine, Xiamen University-Jiangsu Charity Biotech Co., Ltd. (Grant No.: 20233160C0002).

Appendix A. Supplementary data

Supplementary data to this article can be found online at https://doi.org/10.1016/j.jpha.2024.101068.

References

[1] W.A. Alrefai, R.K. Gill, Bile acid transporters: Structure, function, regulation and pathophysiological implications, Pharm. Res. 24 (2007) 1803–1823.
[2] J.L. Thistle, Ursodeoxycholic acid treatment of gallstones, Semin Liver Dis. 3 (1983) 146–156.
[3] A. Parés, L. Caballería, J. Rodés, et al., Long-term effects of ursodeoxycholic acid in primary biliary cirrhosis: results of a double-blind controlled multicentric

trial. UDCA-Cooperative Group from the Spanish Association for the Study of the Liver, J. Hepatol. 32 (2000) 561–566.
[4] T. Brevini, M. Maes, G.J. Webb, et al., FXR inhibition may protect from SARS-CoV-2 infection by reducing ACE2, Nature 615 (2023) 134–142.
[5] L. Pang, X. Zhao, W. Liu, et al., Anticancer effect of ursodeoxycholic acid in human oral squamous carcinoma HSC-3 cells through the caspases, Nutrients 7 (2015) 3200–3218.
[6] F. Wang, C. Qin, Y. Li, et al., Ursodeoxycholic acid induces autophagy via LC3B to suppress hepatocellular carcinoma *in vivo* and *in vitro*, Int. J. Clin. Exp. Pathol. 10 (2017) 11805–11813.
[7] S.C. Lim, H.Q. Duong, J.E. Choi, et al., Lipid raft-dependent death receptor 5 (DR5) expression and activation are critical for ursodeoxycholic acid-induced apoptosis in gastric cancer cells, Carcinogenesis 32 (2011) 723–731.
[8] J.F. Goossens, C. Bailly, Ursodeoxycholic acid and cancer: From chemoprevention to chemotherapy, Pharmacol. Ther. 203 (2019), 107396.
[9] M.H. Stipanuk, J.E. Dominy, Jr. Lee, et al., Mammalian cysteine metabolism: New insights into regulation of cysteine metabolism, J. Nutr. 136 (2006) 1652S–1659S.
[10] A. Meister, Glutathione metabolism, Methods Enzymol. 251 (1995) 3–7.
[11] W.S. Yang, B.R. Stockwell, Ferroptosis: Death by lipid peroxidation, Trends Cell Biol. 26 (2016) 165–176.
[12] C.S. Shin, P. Mishra, J.D. Watrous, et al., The glutamate/cystine xCT antiporter antagonizes glutamine metabolism and reduces nutrient flexibility, Nat. Commun. 8 (2017), 15074.
[13] K. Otsubo, K. Nosaki, C.K. Imamura, et al., Phase I study of salazosulfapyridine in combination with cisplatin and pemetrexed for advanced non-small-cell lung cancer, Cancer Sci. 108 (2017) 1843–1849.
[14] K. Hu, K. Li, J. Lv, et al., Suppression of the SLC7A11/glutathione axis causes synthetic lethality in KRAS-mutant lung adenocarcinoma, J. Clin. Invest. 130 (2020) 1752–1766.
[15] S. Dolma, S.L. Lessnick, W.C. Hahn, et al., Identification of genotype-selective antitumor agents using synthetic lethal chemical screening in engineered human tumor cells, Cancer Cell 3 (2003) 285–296.
[16] M. Sato, K. Onuma, M. Domon, et al., Loss of the cystine/glutamate antiporter in melanoma abrogates tumor metastasis and markedly increases survival rates of mice, Int. J. Cancer 147 (2020) 3224–3235.
[17] J.L. Roh, E.H. Kim, H. Jang, et al., Aspirin plus sorafenib potentiates cisplatin cytotoxicity in resistant head and neck cancer cells through xCT inhibition, Free. Radic. Biol. Med. 104 (2017) 1–9.
[18] G. Gatta, J.M. van der Zwan, P.G. Casali, et al., Rare cancers are not so rare: The rare cancer burden in Europe, Eur. J. Cancer 47 (2011) 2493–2511.
[19] C. Messiou, E. Moskovic, D. Vanel, et al., Primary retroperitoneal soft tissue sarcoma: Imaging appearances, pitfalls and diagnostic algorithm, Eur. J. Surg. Oncol. 43 (2017) 1191–1198.
[20] I. Judson, J. Verweij, H. Gelderblom, et al., Doxorubicin alone versus intensified doxorubicin plus ifosfamide for first-line treatment of advanced or metastatic soft-tissue sarcoma: A randomised controlled phase 3 trial, Lancet Oncol. 15 (2014) 415–423.
[21] X. García-Del-Muro, A. López-Pousa, J. Maurel, et al., Randomized phase II study comparing gemcitabine plus dacarbazine versus dacarbazine alone in patients with previously treated soft tissue sarcoma: A Spanish Group for Research on Sarcomas study, J. Clin. Oncol. 29 (2011) 2528–2533.
[22] C.M. Fletcher, The evolving classification of soft tissue tumours: An update based on the new 2013 WHO classification, Histopathology 64 (2014) 2–11.
[23] Y. Shen, C. Lu, Z. Song, et al., Ursodeoxycholic acid reduces antitumor immunosuppression by inducing CHIP-mediated TGF-β degradation, Nat. Commun. 13 (2022), 3419.
[24] R.E. Poupon, B. Balkau, E. Eschwège, et al., A multicenter, controlled trial of ursodiol for the treatment of primary biliary cirrhosis, UDCA-PBC Study Group, N. Engl. J. Med. 324 (1991) 1548–1554.
[25] E. Ros, S. Navarro, C. Bru, et al., Ursodeoxycholic acid treatment of primary hepatolithiasis in Caroli's syndrome, Lancet 342 (1993) 404–406.
[26] S.E. Jäntti, M. Kivilompolo, L. Ohrnberg, et al., Quantitative profiling of bile acids in blood, adipose tissue, intestine, and gall bladder samples using ultra high performance liquid chromatography-tandem mass spectrometry, Anal. Bioanal. Chem. 406 (2014) 7799–7815.
[27] J.D. Young, INCA: A computational platform for isotopically non-stationary metabolic flux analysis, Bioinformatics 30 (2014) 1333–1335.
[28] A. Roda, G. Cappelleri, R. Aldini, et al., Quantitative aspects of the interaction of bile acids with human serum albumin, J. Lipid Res. 23 (1982) 490–495.
[29] T.H. Murphy, M. Miyamoto, A. Sastre, et al., Glutamate toxicity in a neuronal cell line involves inhibition of cystine transport leading to oxidative stress, Neuron 2 (1989) 1547–1558.
[30] W. Guo, K. Li, B. Sun, et al., Dysregulated glutamate transporter SLC1A1 propels cystine uptake via Xc(-) for glutathione synthesis in lung cancer, Cancer Res. 81 (2021) 552–566.
[31] S. Basu, T. Barnoud, C.P. Kung, et al., The African-specific S47 polymorphism of p53 alters chemosensitivity, Cell Cycle 15 (2016) 2557–2560.
[32] Y. Zhang, R.V. Swanda, L. Nie, et al., mTORC1 couples cyst(e)ine availability with GPX4 protein synthesis and ferroptosis regulation, Nat. Commun. 12 (2021), 1589.
[33] A.P.A. Janssen, J.M.A. van Hengst, O.J.M. Béquignon, et al., Structure kinetics relationships and molecular dynamics show crucial role for heterocycle leaving group in irreversible diacylglycerol lipase inhibitors, J. Med. Chem. 62 (2019) 7910–7922.
[34] M.Y. Cissé, S. Pyrdziak, N. Firmin, et al., Targeting MDM2-dependent serine metabolism as a therapeutic strategy for liposarcoma, Sci. Transl. Med. 12 (2020), eaay2163.
[35] A.P. Dei Tos Liposarcomas, Diagnostic pitfalls and new insights, Histopathology 64 (2014) 38–52.
[36] J. Lu, D. Wood, E. Ingley, et al., Update on genomic and molecular landscapes of well-differentiated liposarcoma and dedifferentiated liposarcoma, Mol. Biol. Rep. 48 (2021) 3637–3647.
[37] F. Xie, Y. Niu, L. Lian, et al., Multi-omics joint analysis revealed the metabolic profile of retroperitoneal liposarcoma, Front. Med. 18 (2024) 375–393.
[38] K. Thway, Well-differentiated liposarcoma and dedifferentiated liposarcoma: An updated review, Semin. Diagn. Pathol. 36 (2019) 112–121.
[39] A. Laroche-Clary, V. Chaire, M.P. Algeo, et al., Combined targeting of MDM2 and CDK4 is synergistic in dedifferentiated liposarcomas, J. Hematol. Oncol. 10 (2017), 123.
[40] B.R. Stockwell, Ferroptosis turns 10: Emerging mechanisms, physiological functions, and therapeutic applications, Cell 185 (2022) 2401–2421.
[41] D. Shin, E.H. Kim, J. Lee, et al., Nrf2 inhibition reverses resistance to GPX4 inhibitor-induced ferroptosis in head and neck cancer, Free Radic. Biol. Med. 129 (2018) 454–462.
[42] A. Okazaki, P.A. Gameiro, D. Christodoulou, et al., Glutaminase and poly(ADP-ribose) polymerase inhibitors suppress pyrimidine synthesis and VHL-deficient renal cancers, J. Clin. Invest. 127 (2017) 1631–1645.
[43] B. Jiang, J. Zhang, G. Zhao, et al., Filamentous GLS1 promotes ROS-induced apoptosis upon glutamine deprivation via insufficient asparagine synthesis, Mol. Cell 82 (2022) 1821–1835.e6.
[44] B. Liu, Y. Chen, D.K. St Clair, ROS and p53: A versatile partnership, Free Radic. Biol. Med. 44 (2008) 1529–1535.
[45] B. Vu, P. Wovkulich, G. Pizzolato, et al., Discovery of RG7112: A small-molecule MDM2 inhibitor in clinical development, ACS Med. Chem. Lett. 4 (2013) 466–469.
[46] C. Tovar, J. Rosinski, Z. Filipovic, et al., Small-molecule MDM2 antagonists reveal aberrant p53 signaling in cancer: Implications for therapy, Proc. Natl. Acad. Sci. USA 103 (2006) 1888–1893.
[47] G. Guney Eskiler, A. Deveci Ozkan, A. Haciefendi, et al., Mechanisms of abemaciclib, a CDK4/6 inhibitor, induced apoptotic cell death in prostate cancer cells *in vitro*, Transl. Oncol. 15 (2022), 101243.
[48] X. Zhu, Z. Fu, K. Dutchak, et al., Cotargeting CDK4/6 and BRD4 promotes senescence and ferroptosis sensitivity in cancer, Cancer Res. 84 (2024) 1333–1351.
[49] J. Zhu, M. Berisa, S. Schwörer, et al., Transsulfuration activity can support cell growth upon extracellular cysteine limitation, Cell Metab. 30 (2019) 865–876.e5.
[50] J. Shukla, K.S. Pitre, Analysis of cystine in human blood for monitoring of cases of burns, J. Pharm. Biomed. Anal. 27 (2002) 821–826.